Published in final edited form as:
Nat Microbiol. 2019 December 01; 4(12): 2246–2259. doi:10.1038/s41564-019-0521-7.

Transcriptome-wide dynamics of extensive m^{6}A mRNA methylation during *Plasmodium falciparum* blood-stage development

Sebastian Baumgarten[1,2,3,*], **Jessica M. Bryant**[1,2,3], **Ameya Sinha**[4,5], **Thibaud Reyser**[1,2,3,7], **Peter R. Preiser**[4,5], **Peter C. Dedon**[5,6], **Artur Scherf**[1,2,3]

[1]Biology of Host–Parasite Interactions Unit, Department of Parasites and Insect Vectors, Institut Pasteur, Paris, France

[2]CNRS, ERL 9195, Paris, France

[3]INSERM, Unit U1201, Paris, France

[4]School of Biological Sciences, Nanyang Technological University Singapore, Singapore, Singapore

[5]Antimicrobial Resistance Interdisciplinary Research Group, Singapore-MIT Alliance for Research and Technology, Singapore, Singapore

[6]Department of Biological Engineering, Massachusetts Institute of Technology, Cambridge, MA, USA

Abstract

Malaria pathogenesis results from the asexual replication of *Plasmodium falciparum* within human red blood cells, which relies on a precisely timed cascade of gene expression over a 48-h life cycle. Although substantial post-transcriptional regulation of this hardwired program has been observed, it remains unclear how these processes are mediated on a transcriptome-wide level. To this end, we identified mRNA modifications in the *P. falciparum* transcriptome and performed a comprehensive characterization of N^6-methyladenosine (m^{6}A) over the course of blood-stage development. Using mass spectrometry and m^{6}A RNA sequencing, we demonstrate that m^{6}A is highly developmentally regulated, exceeding m^{6}A levels known in any other eukaryote. We

[*]**Correspondence and requests for materials** should be addressed to S.B. sebastian.baumgarten@pasteur.fr.
[7]Present address: Laboratoire de Chimie de Coordination, Toulouse, France.

Reporting Summary. Further information on research design is available in the Nature Research Reporting Summary linked to this article.

Author contributions
P.R.P, P.C.D. and A.Sc. conceptualized the project. S.B., J.M.B. and A.Sc. conceived experiments. J.M.B. developed and performed CRISPR interference and dCas9 ChIP-seq experiments. S.B. performed m^{6}A-seq and RT-qPCR experiments. A.Si. performed and analysed LC-MS/MS and protein co-IP experiments. S.B., J.M.B. and T.R. generated constructs, transfectants and parasite material. S.B. performed bioinformatic analyses. P.R.P., P.C.D. and A.Sc. supervised and helped interpret analyses. All authors discussed and approved the manuscript.

Competing interests
The authors declare no competing interests.

Europe PMC Funders Author Manuscripts

characterize a distinct m^{6}A writer complex and show that knockdown of the putative m^{6}A methyltransferase, PfMT-A70, by CRISPR interference leads to increased levels of transcripts that normally contain m^{6}A. In accordance, we find an inverse correlation between m^{6}A methylation and mRNA stability or translational efficiency. We further identify two putative m^{6}A-binding YTH proteins that are likely to be involved in the regulation of these processes across the parasite's life cycle. Our data demonstrate unique features of an extensive m^{6}A mRNA methylation programme in malaria parasites and reveal its crucial role in dynamically fine-tuning the transcriptional cascade of a unicellular eukaryote.

Malaria, a mosquito-borne human disease caused by the unicellular apicomplexan parasite *Plasmodium falciparum*, remains a major global health threat[1]. Human pathogenesis results from the 48-h intra-erythrocytic developmental cycle (IDC), during which each parasite undergoes schizogony within red blood cells (RBCs) to create up to 32 new daughter cells (Fig. 1a). Each step of the IDC—from RBC invasion (0 h post-infection (h.p.i.)) to egress—is effected by a precisely timed cascade of gene expression. Throughout this process, mRNAs from the majority of genes expressed reach peak abundance only once, which is thought to correspond to the time point when its encoded product is most required[2]. While gene silencing is partially achieved via heterochromatinization of genes encoding variant surface antigens[3] and the inducer of sexual stage development[4], the large majority of the *P. falciparum* genome is in a euchromatic and transcriptionally permissive state throughout the IDC[5]. Here, dynamic chromatin accessibility in promoter regions strongly correlates with mRNA abundance, and these sequences can be recognized by transcription factors in vitro[6,7]. While the parasite's periodic profile of mRNA abundance appears to be hardwired and unresponsive to perturbation throughout the IDC[8,9], changes in mRNA turnover have been found to substantially contribute to overall mRNA abundances on top of transcriptional activity during the IDC[10]. Therefore, it has been suggested that while transcription may dictate the initial level of mRNA abundance, modulation at the RNA level could provide a more sensitive and/or responsive layer of regulation[10–12]. Such fine-tuned post-transcriptional regulation in *P. falciparum* is most evident in the dynamics of mRNA degradation rates. mRNA stability was shown to be highly dynamic during the IDC[10] and to increase gradually over a single developmental cycle[13]. Moreover, extensive post-transcriptional repression of protein synthesis occurs throughout the IDC[14], and translational efficiency was found to differ substantially among mRNA transcripts at the same time point during the IDC[15]. However, the underlying mechanisms orchestrating these processes on a transcriptome-wide scale are as yet unknown.

Several recent studies in model organisms have shown that chemical nucleotide modifications located at internal positions of mRNA can act as mediators of global post-transcriptional regulation of gene expression[16]. Most notably, the relatively abundant N^6-methyladenosine (m^{6}A) has been shown to affect a multitude of cellular processes. In mammalian cells, m^{6}A is catalysed by a methyltransferase complex consisting of a catalytically active m^{6}A methyltransferase (METTL3, methyltransferase-like 3), a second methyltransferase-like protein (METTL14) and the METTL3 adaptor protein WTAP (Wilms-tumour-1 associated protein)[17]. METTL14 does not have enzymatic activity by itself[18], but provides the binding site for substrate mRNA and allosterically induces

the activity of METTL3[19]. A key function of WTAP is the localization of the m^{6}A 'writer' complex to nuclear speckles[20]. While other proteins can assemble with the m^{6}A methyltransferase complex in mammalian cells, orthologues of METTL3, METTL14 and WTAP form an evolutionarily conserved m^{6}A core complex among eukaryotes[17].

m^{6}A can change the secondary structure of RNAs[21], making adjacent binding sites accessible for RNA-binding proteins (RBPs), or directly recruit specific m^{6}A-binding proteins[17]. In mammalian cells, m^{6}A-binding proteins include proteins of the YTH (YT521-B homology) family and eIF3 (eukaryotic initiation factor 3). m^{6}A-mediated recruitment of eIF3 initiates translation independent of the canonical cap-binding eIF4E[22], whereas YTHDF (YTH domain family) proteins can decrease mRNA stability[23] and enhance translation[24]. The cellular and organismal processes affected by m^{6}A are widespread and include cell differentiation and cancer cell progression in mammalian cells[25], sex determination in *Drosophila* [26], and meiosis in yeast[27].

The *P. falciparum* genome has the highest AT content (~80%) of any organism sequenced so far[28]. More intriguing yet is the even stronger adenosine bias in the mRNA transcriptome, with adenosines constituting ~45% of all mRNA nucleotides, compared to ~32% in yeast or ~27% in humans. The reason for this high AT bias remains puzzling, but given this unique nucleotide composition and high level of post-transcriptional regulation during the IDC, we hypothesized that mRNA nucleotide modifications, especially on adenosines, could provide an additional layer of gene regulation in *P. falciparum*.

Here, we use mass spectrometry to identify *P. falciparum* mRNA modifications and show that m^{6}A mRNA methylation is a crucial layer of post-transcriptional regulation during the IDC. We identify unique features of the parasite's methylation program, including a distinct m^{6}A writer complex, preferential m^{6}A site localization, m^{6}A-mediated translational repression and a diverse set of putative m^{6}A-binding proteins. Using CRISPR interference, we characterize the methyltransferase PfMT-A70 as an integral component in m^{6}A methylation and show that m^{6}A dynamically fine-tunes a hardwired transcriptional program across *P. falciparum* blood-stage development.

Results

Identification of a dynamic m^{6}A methylation program during *P. falciparum* blood-stage development

We first identified mRNA modifications in an unbiased manner with chromatography-coupled triple quadrupole mass spectrometry (LC-MS/MS) from synchronized parasites harvested over the course of the IDC (Supplementary Fig. 1a,b). Ten modifications previously identified in eukaryotic mRNAs were detected in our analysis over the course of the IDC (Fig. 1b,c and Supplementary Fig. 1c,d). These modifications include N^7-methylguanosine (m^{7}G), pseudouridine (Ψ), 5-methylcytidine (m^{5}C), and N^6-methyladenosine (m^{6}A) (Supplementary Table 1 and Fig. 1d). m^{6}A was previously reported to be the most abundant internal mRNA modification in mammalian cells[16]. While global m^{6}A/A levels in *P. falciparum* are comparable to those in human mRNA (Fig. 1e and Supplementary Table 2), overall m^{6}A levels in the parasite's mRNA (45% adenosine) are

higher throughout almost the entire IDC (Fig. 1e). Moreover, m^6A mRNA methylation in *P. falciparum* is highly developmentally regulated, with a continuous increase from 0.3% at early stages of the IDC up to 0.7% m^6A/A at 30 h.p.i. (Fig. 1e and Supplementary Fig. 1e).

The *P. falciparum* genome encodes a highly conserved putative orthologue (PF3D7_0729500) of the m^6A mRNA methyltransferase[18] characterized in other eukaryotes (METTL3 in mammalian cells, Ime4 in *Saccharomyces cerevisiae*, and MTA in *Arabidopsis thaliana*) (Fig. 2a). The encoded protein contains the functional domain of its putative orthologues (MT-A70) and has been designated PfMT-A70. To investigate a potentially conserved role in *P. falciparum*, we generated a cell line expressing an HA-tagged PfMT-A70 protein, which localized to the nucleus and the cytoplasm (Fig. 2b).

We next performed immunoprecipitation of PfMT-A70-HA followed by LC-MS and identified 16 specific proteins (Fig. 2c,d and Supplementary Table 3), one of which (PF3D7_1230800) is highly conserved with eukaryotic orthologues of WTAP (Fig. 2d and Supplementary Fig. 2a). The *P. falciparum* orthologue contains a WTAP/MUM2 domain and was designated PfWTAP. We identified a second putative mRNA methyltransferase containing an MT-A70 domain (PF3D7_1235500, designated PfMT-A70.2) that shows high sequence conservation with orthologues of the bilaterian METTL14 (Fig. 2d and Supplementary Fig. 2a). All three *P. falciparum* orthologues reach peak transcription levels between 12 and 24 h.p.i., shortly before maximal m^6A/A ratios are reached (Figs. 1e and 2e). Among the other co-immunoprecipitated proteins are known RNA/DNA binding proteins such as Alba3, an ATP-dependent RNA helicase, and a FoP-domain-containing protein. Three proteins identified with high confidence (PF3D7_0707200, PF3D7_1036900 and PF3D7_1366300) have unknown functions and show no homology to other eukaryotic proteins (Supplementary Table 3).

CRISPR interference of PfMT-A70 decreases global m^6A mRNA methylation

We targeted PfMT-A70 to gain insight into the functional role of m^6A mRNA methylation in *P. falciparum*. As attempted CRISPR/Cas9-targeted deletion was unsuccessful, we utilized CRISPR interference[29] (CRISPRi; Supplementary Fig. 2b), which has recently been adapted for *P. falciparum* [30]. For CRISPRi of PfMT-A70, we targeted its promoter downstream of the transcription start site and ~100 bp upstream of the translation start site with a gRNA complementary to the non-template strand (‘gPfMT-A70’, Fig. 3a). A cell line expressing a non-specific gRNA served as a negative control (‘gControl’, Fig. 3a). gPfMT-A70-targeted dCas9 chromatin immunoprecipitation followed by sequencing (ChIP-seq)[31] showed a robust and highly specific enrichment at the target site, which overlaps with a nucleosome-depleted region (FAIRE)[32] enriched for H3K9ac[5] and H2A.Z[33] (that is, hallmarks of promoter regions in *P. falciparum* [34]; Fig. 3b,c).

To determine the effects of PfMT-A70 CRISPRi, we harvested mRNA from synchronized gPfMT-A70 and gControl parasites at 12, 24 and 36 h.p.i. RT-qPCR revealed a significant downregulation of PfMT-A70 transcripts throughout the IDC, with knockdown levels ranging from ~15% at 12 h.p.i. to 40% at 24 and 36 h.p.i. (Fig. 3d, top). While PfMT-A70 CRISPRi did not have a discernible effect on parasite growth (Supplementary Fig. 2c), LC-MS/MS revealed a significant 10–30% decrease in global m^6A/A levels at all three time

points (Fig. 3d, bottom), further identifying PfMT-A70 as an integral component of the m^{6}A writer complex in *P. falciparum*.

mRNA transcripts are differentially m^{6}A-methylated during the IDC

We measured the dynamics of m^{6}A mRNA methylation on a transcript-specific level across the IDC using m^{6}A-methylated mRNA immunoprecipitation (IP) followed by sequencing (m^{6}A-seq) (Supplementary Fig. 2d,e). m^{6}A-IP followed by LC-MS/MS demonstrated high antibody specificity (Fig. 4a and Supplementary Fig. 2f). We next prepared strand-specific RNA sequencing libraries from m^{6}A eluates ('m^{6}A-IP') and mRNA input ('m^{6}A-input', used for peak normalization) from two replicates of gPfMT-A70 and gControl parasites at 12, 24 and 36 h.p.i. More than 99% of reads map to protein-coding regions, confirming that the m^{6}A LC-MS/MS measurements result from mRNA and not ribosomal or transfer RNAs.

We stringently mapped m^{6}A methylation sites in gPfMT-A70 and gControl samples (two replicates each) collected at 12, 24 and 36 h.p.i. We identified 603, 873 and 996 significant m^{6}A peaks at 12, 24 and 36 h.p.i., which parallels the global increase in m^{6}A/A levels as measured by LC-MS/MS. At all time points, the majority of transcripts contain only one m^{6}A peak (Supplementary Fig. 3a) with an average of ~0.7 m^{6}A peaks per kilobase of exon (Supplementary Fig. 3b). The main determinant of m^{6}A peak number per transcript is transcript length: transcripts with two or more peaks are ~70% longer than transcripts with a single m^{6}A peak. In total, we identified 1,520 non-overlapping m^{6}A peaks across all time points, present in 1,043 distinct transcripts (Supplementary Tables 4–6). 256 peaks located in 205 distinct transcripts were identified at all three time points independently. These transcripts are enriched in functions related to RNA processing ($Q = 8.5 \times 10^{-3}$) and include multiple pre-mRNA splicing factors (Supplementary Table 7).

m^{6}A peak summits are almost exclusively ($n = 1{,}514$) found within protein-coding sequences or 200 nucleotides (nt) upstream of the translation start or downstream of the translation stop site. While five m^{6}A peaks were identified in intergenic regions and one in an intron, no enrichment of m^{6}A peaks was observed near intron–exon boundaries (Supplementary Fig. 3c). In contrast to the topology of m^{6}A sites in metazoans and plants, m^{6}A peaks in *P. falciparum* are not enriched near the stop codon and 3' UTR, but show a tendency for localization towards the 5' end (Fig. 4b,c).

We searched for sequence motifs associated with m^{6}A peaks and found a GGACA motif to be most significantly enriched ($P = 1 \times 10^{-12}$; Supplementary Table 8). This motif is similar to the RGAC and DRACH (D = G/A/U; R = G/A; H = C/A/U) motifs identified at yeast[27] and human m^{6}A sites[35] (Fig. 4d). Compared to a control sequence set of similar length and size, motifs in an RAC context are generally enriched (Supplementary Fig. 3d), with the deduced consensus motif occurring in 87% of all m^{6}A peaks. Similar to m^{6}A peaks, the motif occurs twice as often within the CDS compared to the highly AT-rich 5' and 3' UTRs (Supplementary Fig. 3e). This motif is also centrally enriched in a region ±20 nt around the m^{6}A peak summit (Fig. 4e), suggesting a certain context dependency for specific m^{6}A methylation.

Europe PMC Funders Author Manuscripts

For an inherently dynamic transcriptional program such as that underlying the IDC of *P. falciparum*, changes in transcript-specific methylation might provide a means of modulating the transcriptome independently of initial gene transcription. Throughout the IDC, there is a modest increase in the total number of transcribed genes that have at least one m^6A peak (Fig. 4f). However, the m^6A enrichment (that is, m^6A-IP/m^6A-input), or fraction of transcripts from one gene containing a specific m^6A peak, changes extensively throughout the IDC (Fig. 4g). Most m^6A peaks reach maximum m^6A enrichment at only one time point, suggesting that transcriptspecific methylation is indeed an actively regulated mechanism.

m^6A inversely correlates with mRNA stability and translational efficiency

To determine the effect of m^6A on individual transcripts, we first compared m^6A enrichment of individual m^6A peaks between gControl and gPfMT-A70 parasites and found a significant reduction in the gPfMT-A70 cell line (Fig. 5a,b, top) at all three time points, mirroring the decrease in global m^6A/A levels in gPfMT-A70 parasites as measured by LC-MS/MS (Fig. 3d, bottom). These decreases are consistent, with two replicates each of gControl and gPfMT-A70 showing a high degree of correlation at each time point (Fig. 5b, bottom, and Supplementary Tables 4–6).

We performed strand-specific mRNA sequencing in gControl and gPfMT-A70 parasites at 12, 24 and 36 h.p.i. and observed minimal changes in global transcript abundance following PfMT-A70 knockdown, with only a small percentage of genes showing significant differential expression (Supplementary Tables 9 and 10). However, at 12 and 24 h.p.i., we found a significant increase in overall abundance of transcripts that show the most pronounced decrease in m^6A enrichment (≥two-fold) following PfMT-A70 depletion (Fig. 5c).

Theoretically, this observed increase in transcript abundance following PfMT-A70 knockdown could be due either to higher transcription rates or lower transcript degradation rates. Because m^6A methylation was previously shown to affect mRNA degradation[23], we compared mRNA stability data (measured as mRNA half-life) previously obtained from wild-type parasites[13] between m^6A-methylated and non-methylated transcripts found in our study. Strikingly, m^6A-methylated transcripts have significantly lower mRNA stabilities than non-methylated transcripts (Fig. 6a, left). These differences are significant at 12 ($P = 5.3 \times 10^{-5}$) and 24 h.p.i. ($P = 9.1 \times 10^{-9}$), but not at the 36 h.p.i. time point ($P = 0.59$). We found even lower mRNA stabilities for the 'm^6A-sensitive' transcripts (≥two-fold decrease in m^6A enrichment and increased transcript abundance ($\log_2$ fold-change >0)) at 12 and 24 h.p.i. (Fig. 6a, right). These data suggest that the increase of transcript abundances following PfMT-A70 knockdown might indeed reflect decreased rates of m^6A-mediated mRNA degradation at the 12 and 24 h.p.i. time points. A further comparison of m^6A methylation with additional mRNA stability data[10] revealed a similar pattern, showing lower mRNA stabilities for m^6A-methylated than non-methylated transcripts (Supplementary Fig. 4a).

We next compared translational efficiencies (TE) between m^6A-methylated and non-methylated transcripts throughout the IDC. TEs were calculated previously for *P. falciparum* as the ratio of ribosome-bound RNA versus steady state mRNA[15]. At each developmental

stage, m^{6}A methylation correlates with significantly lower translational efficiencies for a transcript (Fig. 6b, left). This correlation is most pronounced at the 12 ($P = 4.7 \times 10^{-9}$) and 24 h.p.i. ($P = 5 \times 10^{-7}$) time points, but is still significant at 36 h.p.i. ($P = 1.5 \times 10^{-3}$). Similarly to the pattern seen for mRNA stability, we observed an additional significant decrease in translational efficiencies between m^{6}A-methylated and the subset of 'm^{6}A-sensitive' transcripts at 12 and 24 h.p.i. (Fig. 6b, right). Notably, the 'm^{6}A-sensitive' transcripts show no preference for m^{6}A peak location across the coding sequence (Supplementary Fig. 4b)

A GO enrichment analysis of the 'm^{6}A-sensitive' transcripts shows that these are enriched for biological processes that are highly relevant for their respective time points of development. At 12 h.p.i., these processes include regulation of gene expression ($Q = 3 \times 10^{-3}$), DNA-templated transcription and regulation of RNA biosynthesis ($Q = 3 \times 10^{-3}$). Among these gene transcripts are four members of the AP2 transcription factor family, two histone deacetylases, one histone-lysine methyltransferase, and one bromodomain-containing protein (Supplementary Table 11). At 24 h.p.i., binding to chromatin ($Q = 6.1 \times 10^{-3}$) is among the most significantly enriched molecular functions, including SNF2 helicases and two SET- and one bromodomain-containing protein (Supplementary Table 11).

P. falciparum encodes an evolutionarily conserved, diverse set of putative m^{6}A-binding proteins

In several eukaryotes, proteins containing a YTH domain have been identified as specific m^{6}A 'reader' proteins, mediating both mRNA degradation and translational activation in an m^{6}A-dependent manner[24]. The *P. falciparum* genome encodes two distinct proteins containing a YTH domain: PfYTH.1 (PF3D7_1419900, previously annotated as 'cleavage and polyadenylation specificity factor subunit 4, CPSF4)[36] and PfYTH.2 (PF3D7_0309800, Fig. 6c). The YTH domain of both proteins shows high conservation of key residues known to bind mRNA and the methylated adenosine in other eukaryotes[24] (Supplementary Fig. 4c). PfYTH.1 also features the C-terminal arrangement of the YTH domain and an N-terminal low-complexity disordered region that is characteristic of metazoan YTHDF proteins (Supplementary Fig. 4d)[24]. In contrast, PfYTH.2 does not show overall similarity to other known m^{6}A reader proteins. Both proteins are highly expressed early during the IDC (Fig. 6d), and ectopic expression of PfYTH.1 revealed localization of the protein to both the nucleus and cytoplasm (Fig. 6e). In comparison to the dynamic expression during the IDC, PfYTH.2 shows even higher expression in the transmission stages of the parasite, namely gametocytes and salivary gland sporozoites, the latter of which also highly expresses PfMT-A70 (Fig. 6d).

Discussion

In this study, we characterize a dynamic and extensive m^{6}A mRNA methylation program that fine-tunes the transcriptional cascade during blood-stage development of *P. falciparum*. We generated a high-resolution map of m^{6}A methylation sites throughout the IDC and identify PfMT-A70 as an integral member of the putative m^{6}A-methyltransferase complex.

Although gene knockout was unsuccessful, CRISPRi allowed us to reduce PfMT-A70 transcript levels to observe consistently decreased m^{6}A levels via LC-MS/MS and m^{6}A-seq, as well as increased abundance of transcripts with decreased m^{6}A enrichment. Higher knockdown levels might be possible with multiple gRNAs, and reveal an effect on parasite growth or more drastic changes in global transcript abundances. However, even using a dCas9-repressor fusion protein did not achieve higher knockdown efficiencies of an essential gene in *P. falciparum* [30]. Thus, it is likely that long transfection and cloning periods favour transgenic clones with lower knockdown levels and possibly lower phenotypic defects. Notably, knockdown or even knockout of the m^{6}A-methyltransferase in *D. melanogaster* [26] or mouse cells[37], respectively, resulted in only moderate changes in gene expression.

The *P. falciparum* m^{6}A methylation program is set apart from those in other eukaryotes by several key aspects. First, while MT-A70 methyltransferases can be found throughout eukaryotes[38] and the core members of the *P. falciparum* m^{6}A writer complex are conserved, we did not identify other co-factors that are similarly conserved in metazoans and plants (for example, HAKAI and VIRMA[39–41]) in our PfMT-A70 co-immunoprecipitation. Thus, the putative *P. falciparum* co-factors are likely to be lineage-specific, and several of them do not share any sequence homology to other eukaryotic proteins. In line with this divergence of the extended m^{6}A writer complex, we find that the m^{6}A motif differs from those found in other eukaryotes[27,35], showing a higher prevalence of adenosine at positions −1 and +2 that mirrors the higher adenosine content of the parasite's mRNA transcriptome. Most identified co-factors show nuclear localization or are found exclusively in the nuclear proteome[42] (for example, PfMT-A70.2), suggesting that m^{6}A methylation in *P. falciparum* occurs prior to nuclear mRNA export. Unlike in other eukaryotes, there is no preference for m^{6}A methylation sites close to the stop codon and the 3' UTR in *P. falciparum*. It was proposed that this 3' enrichment largely depends on the protein VIRMA, which in mammalian cells specifically recruits the m^{6}A writer complex to the 3' UTR[43]; however, we did not identify an orthologue in the *P. falciparum* genome.

With the high adenosine content in the parasite's protein-coding transcriptome, overall m^{6}A levels markedly exceed those measured in human mRNA, suggesting a key role for this modification during asexual replication. It is tempting to speculate that m^{6}A methylation might represent one evolutionary driving force of high adenosine content observed at gene loci. In addition, the functional diversity of transcripts containing m^{6}A suggests that this modification is involved in various important cellular processes during the IDC. While m^{6}A may directly affect the fate of an mRNA transcript and its encoded protein, the modulation of transcripts encoding major regulatory proteins such as AP2 transcription factors or chromatin remodellers might further amplify its modulatory potential.

In mammalian cells, m^{6}A levels are mostly static even during key developmental stages such as stem cell differentiation[39,44], with deregulation of METTL3 and increases in global m^{6}A of only 25% being sufficient to inhibit differentiation, promote cell growth, and maintain tumorigenicity[25]. Although the m^{6}A-demethylases Alkbh5 and FTO may modulate methylation levels in some cases[17], m^{6}A is generally deposited early and maintained throughout the life of an mRNA transcript[45]. In contrast, the most unique feature of the *P. falciparum* m^{6}A methylation program is its dynamic nature. Parallel LC-MS/MS

measurements and transcript-specific m^{6}A-seq demonstrated similar m^{6}A dynamics, with global m^{6}A/A levels doubling and the number of identified m^{6}A peaks gradually increasing towards the end of the IDC. Since we did not find a potential m^{6}A demethylase in the *P. falciparum* genome, m^{6}A methylation dynamics during the IDC could result from different rates of active m^{6}A methylation by the writer complex and the subsequent rate of m^{6}A-methylated transcript degradation. Indeed, the observed gradual increase of global m^{6}A/A levels measured by LC-MS/MS might be partially due to the m^{6}A-mediated mRNA degradation at earlier but not later stages of the IDC, as is evidenced by the inverse correlation of m^{6}A status and mRNA stability at 12 and 24 h.p.i., but not 36 h.p.i It follows that transcripts with decreased m^{6}A enrichment are overabundant at only the earlier (and not the late) time point following PfMT-A70 depletion.

These differences in m^{6}A-dependent mRNA degradation rates might be due to m^{6}A reader proteins mediating mRNA turnover. Both PfYTH.1 and PfYTH.2 transcription decreases over the course of the IDC (Fig. 6d), providing a potential link between the gradual increase in global m^{6}A/A levels and the decrease in m^{6}A-mediated transcript degradation over the course of parasite development. Similarly, we find the strongest association between m^{6}A and translational efficiency at 12 h.p.i., with a continuous decrease during the IDC (Fig. 6b, left). Thus, the timely action of m^{6}A writers and the combinatorial or exclusive expression of putative reader proteins tightly regulate m^{6}A dynamics, probably ensuring the maximal modulatory potential of m^{6}A at each step of the lifecycle.

Mammalian YTHDF proteins 1 to 3 have been linked to mRNA degradation and translational activation[24]. However, based on their sequence similarity and the overlap of binding sites[46], it was suggested that these proteins might be partially redundant[17]. In contrast, *P. falciparum* encodes only two YTH proteins, and while their roles are unknown, the divergence of these two proteins beyond their YTH domain and the distinct expression patterns during the parasite lifecycle suggest that they mediate two distinct functions. m^{6}A has not been associated with translational repression in any eukaryote yet, but this post-transcriptional regulation is of particular importance for *P. falciparum* during the IDC[15] and especially during transmission between the human host and mosquito vector[47,48]. During the latent gametocyte and salivary gland sporozoite stages, mRNAs are kept in a translationally repressed state and protein synthesis is only initiated following transmission, readily ensuring rapid continuation of development[12,49]. The co-expression of PfMT-A70 and PfYTH.2 in sporozoites suggests that m^{6}A could also contribute to translational repression during this transmission stage (Fig. 6d).

The major factor controlling mRNA transcript abundance during the IDC is certainly the transcriptional activity at the genic locus[7,10]. However, here we show that the fate of individual transcripts from the same gene can be changed, possibly by decreasing mRNA stability and/or repressing translation through specific m^{6}A methylation. Our findings that (1) transcripts with decreased m^{6}A enrichment following PfMT-A70 knockdown were consistently more abundant and (2) there is an increased association between ‘m^{6}A-sensitivity’ and mRNA stability and translational repression suggest that m^{6}A serves as a balance to modulate the outcome of protein synthesis independent of initial transcriptional rates. Thus, temporally dynamic changes of transcript-specific m^{6}A methylation rates during

the IDC have, to a certain extent, the potential to finetune a possibly imprecise, hardwired transcriptional program.

Collectively, our study reveals an additional layer of dynamic and widespread post-transcriptional modulation of gene expression in *P. falciparum*. The conservation of core features of m^6A mRNA methylation makes *P. falciparum* an excellent system to study the interplay between m^6A methylation and gene transcription. Moreover, our results add m^6A as a major player in the malaria parasite 'epitranscriptome' code and open new avenues for drug development in malaria parasites.

Methods

Parasite culture

Asexual blood-stage *P. falciparum* parasites (strain 3D7) were cultured as described previously[50]. Briefly, parasites were cultured in human RBCs in RPMI-1640 culture medium (Thermo Fisher no. 53400-025) supplemented with 10% v/v Albumax I (Thermo Fisher no. 11020039), hypoxanthine (0.1 mM final concentration, CC-Pro no. Z-41-M) and 10 mg gentamicin (Sigma no. G1397-10ML) at 4% haematocrit and under 5% O_2, 3% CO_2 at 37 °C. Parasite development was monitored by Giemsa staining. RBCs were obtained from the Etablissement Français du Sang with approval number HS 2016-24803.

For synchronization, late stage parasites were enriched with plasmagel flotation followed by ring stage enrichment via sorbitol (5%) lysis 6 h later. For sampling of highly synchronous parasites during the IDC, the synchronous schizonts were enriched by plasmagel flotation shortly before reinvasion, followed by a sorbitol lysis 6 h later. The 0 h time point was considered to be 3 h after plasmagel flotation. Parasites were collected at 4% haematocrit and ~2–3% parasitaemia.

Parasite growth assay

Parasite growth kinetics were measured as described previously[51]. Briefly, two clones of gControl and gPfMT-A70 *P. falciparum* parasites were tightly synchronized and diluted to 0.2% parasitaemia at ring stage (0 h). The growth curve was replicated in three distinct batches of RBCs on a 96-well plate (200 µl complete culture media per well). Parasitaemia was measured every 24 h by staining parasite nuclei using SYBR Green I (Sigma no. S9430) and counting (un-) infected RBCs using a Guava easyCyte flow cytometer (Merck Millipore).

Total RNA extraction

For RNA extraction, infected RBCs (iRBCs) were collected by centrifugation and washed once with Dulbecco's phosphate-buffered saline (DPBS) (Thermo Fisher no. 14190-144) at 37 °C. iRBCs were lysed in 0.075% saponin in DPBS at 37 °C, and the parasite cell pellet was washed once with DPBS and then resuspended in 700 µl QIAzol reagent (Qiagen no. 79306). Total RNA was extracted using the miRNeasy Mini Kit (Qiagen no. 217004), including an on-column DNase I digestion and exclusion of small RNA (<200 nt) according to the manufacturer's protocol.

Analysis of mRNA modifications by LC-MS/MS

Total RNA from highly synchronous parasites was extracted from samples collected during the IDC at seven time points at 6-h intervals (that is, 6 h.p.i. to 42 h.p.i.). To minimize human RNA and DNA contamination, parasites were cultured in leukocyte-depleted RBCs. Total RNA from human A549 cells was extracted as described above. Poly(A) RNA from *P. falciparum* or human A549 total RNA was enriched by two successive rounds of purification with the Dynabeads mRNA purification kit (Thermo Fisher no. 61006) (Supplementary Fig. 1b).

Purified *P. falciparum* RNA was hydrolysed enzymatically as described with a slightly modified protocol using the following components in the buffer mix (10 mM Tris-HCl (pH 7.9), 1 mM $MgCl_2$, 5 U benzonase (Merck no. 71206), 50 µM desferroxamine (Sigma no. D9533), 0.1 µg $µl^{-1}$ pentostatin (Sigma no. SML0508), 100 µM butylated hydroxytoluene (Sigma no. W218405), 0.5 µg $µl^{-1}$ tetrahydrouridine (Calbiochem no. 584222), 5 U bacterial alkaline phosphatase (Thermo Fisher no. 18011015), 0.05 U phosphodiesterase I (Sigma no. P3243)) and $[^{15}N]_5$-2'-deoxyadenosine ($[^{15}N]$-dA) (Cambridge Isotope Laboratories no. NLM-3895-25) as the internal standard to account for variations in sample handling and mass spectrometer response[52]. Hypersil GOLD aQ column (100 × 2.1 mm, 1.9 µm (Thermo Scientific no. 25305)) was used to resolve the digested ribonucleosides in a two-buffer eluent system (buffer A = 0.1% formic acid in water; buffer B = 0.1% formic acid in acetonitrile). HPLC was performed at a flow rate of 300 µl m^{-1} at 25 °C. The gradient of 0.1% formic acid in acetonitrile was as follows: 0–12 min, held at 0%; 12–15.3 min, 0–1%; 15.3–18.7 min, 1–6%; 18.7–20 min, held at 6%; 20–24 min, 6–100%; 24–27.3 min, held at 100%; 27.3–28 min, 100–0%; 28–41 min, 0%. The HPLC column was directly connected to an Agilent 6490 triple quadrupole mass spectrometer or Agilent 6530 q-ToF with ESI Jetstream ionization operated in positive ion mode. The voltages and source gas parameters were as follows: gas temperature, 50 °C; gas flow, 11 l min^{-1}; nebulizer, 20 psi; sheath gas temperature, 300 °C; sheath gas flow, 12 l min^{-1}; capillary voltage, 1,800 V; and nozzle voltage, 2,000 V. The molecular transition ions were quantified in multiple-reaction monitoring (MRM) mode (Supplementary Table 1). For the collision-induced dissociation using the q-ToF, data was acquired from 200–500 m/z with an acquisition rate of 5 spectra s^{-1} in MS mode and from 50 to 500 m/z with an acquisition rate of 2 spectra s^{-1} in MS/MS mode.

Generation of tagged PfMT-A70 and PfYTH *P. falciparum* strains

PfMT-A70 and PfYTH open reading frames (ORF) without stop codon were PCR-amplified from *P. falciparum* genomic DNA (strain 3D7) using primers MT-A70_F/MT-A70_R and YTH1_F/YTH1-R (Supplementary Table 12), respectively. A 3×FLAG-2×HA tag was synthesized by GenScript (Piscataway, USA) and PCR-amplified using the primer pair MT-A70_HA-F/HA_R for PfMT-A70 and YTH1_HA-F/HA_R for PfYTH (Supplementary Table 12). The resulting tag fragments were fused to the C terminus of the corresponding ORF fragment with PCR using primer pairs MT-A70_F/HA_R for PfMT-A70 and YTH1_F/HA_R for PfYTH (Supplementary Table 12). The final PCR fragments were cloned into the XhoI/KpnI restriction sites of the pARL-STEVOR^{full} vector backbone[53] using the In-Fusion HD cloning kit (Clontech no. 639649). The resulting plasmids were verified

by Sanger sequencing. All PCR reactions were performed using the KAPA HiFi DNA Polymerase (Roche no. 07958846001) following the manufacturer's protocol, but with lower elongation temperature (62 °C or 68 °C). Cloning and plasmid amplification were performed using XL10-Gold ultracompetent *E. coli* (Agilent Technologies no. 200315) following the manufacturer's protocol. The final plasmids (pARL-PfMT-A70-3×FLAG-2×HA and pARL-PfYTH-3×FLAG-2×HA) contain the drug-selectable marker human dihydrofolate reductase (hDHFR), conferring resistance to the antifolate drug WR99210. The final plasmids encode a full length PfMT-A70 or PfYTH protein with a C-terminal 3×FLAG-2×HA tag under the chloroquine resistance transporter promoter (Supplementary Fig. 2b).

Ring-stage parasites were transfected with 50 μg plasmid by electroporation as described previously[54] and drug-resistant parasites emerged after four weeks of continuous culture in the presence of 2.67 nM WR99210 (Jacobus Pharmaceuticals).

Protein fractionation and western blot analysis

One ml iRBCs containing synchronous parasites expressing HA-tagged PfMT-A70 or PfYTH at ring stage (2–3% parasitaemia) were washed once with DPBS at 37 °C, and RBCs were lysed with 0.075% saponin in DPBS. Parasites were then washed once again with DPBS. For separation of the cytoplasmic and nuclear protein fractions, the cell pellet was first resuspended in 1 ml cytoplasmic lysis buffer (CLB: 25 mM Tris-HCl pH 7.5, 10 mM NaCl, 1% IGEPAL CA-630, 1 mM DTT, 1.5 mM $MgCl_2$, 1× protease inhibitor (PI, Roche no. 11836170001)) and incubated on ice for 30 min. Cells were further homogenized in a glass douncer, and the cytoplasmic lysate was cleared with centrifugation (13,500*g*, 10 min, 4 °C). The pellet (containing the nuclei) was resuspended in 100 μl nuclear extraction buffer (25 mM Tris-HCl pH 7.5, 1 mM DTT, 1.5 mM $MgCl_2$, 600 mM NaCl, 1% IGEPAL CA-630, PI) supplemented with 1 μl benzonase (Sigma Aldrich no. E1014-5KU) and sonicated for 10 cycles with 30 s (on/off) intervals (5 min total sonication time) in a Diagenode Bioruptor Pico (Diagenode no. B01060010). This nuclear lysate was cleared with centrifugation (13,500*g*, 10 min, 4 °C), and the nuclear fraction was diluted with 300 μl CLB.

Protein samples were supplemented with NuPage Sample Buffer (Thermo Fisher no. NP0008) and NuPage Reducing Agent (Thermo Fisher no. NP0004) and denatured for 10 min at 70 °C. The samples were separated on a NuPage 4–12% Bis-Tris gel using MOPS running buffer at 150 V for 1.5 h and transferred to a PVDF membrane overnight at 15 V at 4 °C. The membrane was blocked for 1 h in 1% milk in 0.1% Tween20 in PBS (PBST). The HA-tagged proteins and histone H3 were detected with anti-HA (Abcam no. ab9110; 1:1,000 in 1% milk-PBST) and anti-H3 (Abcam no. ab1791: 1:1,000 in 1% milk-PBST) primary antibodies, respectively, followed by donkey anti-rabbit (GE no. NA934-1ML) secondary antibodies conjugated to HRP (1:5,000). PfAldolase was detected using an HRP conjugated anti-PfAldolase (Abcam no. ab38905, 1:5,000 in 1% milk PBST) antibody. The HRP signal was developed using the SuperSignal West Pico chemiluminescent substrate (Thermo Fisher no. 34580) and imaged with a ChemiDoc XRS+ (Bio-Rad).

PfMT-A70 co-immunoprecipitation

P. falciparum PfMT-A70-HA (n = 3 replicates) expressing parasites (cultured with 2.67 nM WR99210 (Jacobus Pharmaceuticals)) and wild-type *P. falciparum* 3D7 (as a negative control, cultured in standard growth medium) were sorbitol-synchronized. After 36 h, the parasites were harvested after Percoll (Sigma no. P4937) enrichment, washed twice with RPMI and crosslinked with 0.5 mM dithiobissuccinimidyl propionate (DSP) (Thermo Fisher no. 22585) in PBS for 60 min at 37 °C[55]. The reaction was quenched with PBS containing 25 mM Tris-HCl. These trophozoites were lysed with RIPA buffer (10 mM Tris HCl pH 7.5, 150 mM NaCl, 0.1% SDS, 1% Triton) containing protease and phosphatase inhibitor cocktail (Thermo Fisher no. 78440). The lysates were cleared by centrifugation at 16,000 *g* for 10 min. Supernatants were incubated with 25 µl of anti-HA Dynabeads (Thermo Fisher no. 88836) overnight at 4 °C. 20 µl of sample were taken prior to separation of the beads for Western blot analysis ('Input', Fig. 2c and Supplementary Fig. 5). Beads were magnetically isolated and 20 µl of sample were taken from the supernatant for Western blot analysis ('Supernatant', Fig. 2c and Supplementary Fig. 5). The beads were washed five times with 1 ml RIPA buffer following five washes with 1 ml PBS and one wash with 1 ml 100 mM ammonium bicarbonate (Sigma no. 09830). The beads were reduced with 10 mM dithiothreitol (Sigma no. D9779), alkylated with 55 mM iodoacetamide (Sigma no. I1149) and subjected to on-bead digestion using 50 µg of trypsin (Thermo Fisher no. 90059). The resulting peptides were desalted using C18 cartridges (Thermo Fisher no. 89852) and sent for MS analysis.

Protein mass spectrometry

Peptides were separated by reverse phase HPLC (Thermo Easy nLC1000) using a precolumn (made in house, 6 cm of 10 µm C18) and a self-pack 5 µm tip analytical column (12 cm of 5 µm C18, New Objective) over a 150 minute gradient before nanoelectrospray using a Q-Exactive HF-X mass spectrometer (Thermo Scientific). The mass spectrometer was operated in a data-dependent mode. The parameters for the full scan MS were: resolution of 70,000 across 350–2000 m/z, AGC $3e^6$, and maximum IT 50 ms. The full MS scan was followed by MS/MS for the top 15 precursor ions in each cycle with a NCE of 28 and dynamic exclusion of 30 s. Raw mass spectral data files (.raw) were searched using Proteome Discoverer (Thermo Fisher) and Mascot (version 2.4.1)[56]. Mascot search parameters were: 10 ppm mass tolerance for precursor ions; 15 milli mass units for fragment ion mass tolerance; two missed cleavages of trypsin; fixed modification was carbamidomethylation of cysteine; variable modifications were methionine oxidation and serine, threonine and tyrosine phosphorylation. Only peptides with a Mascot score greater than or equal to 25 and an isolation interference less than or equal to 30 were included in the data analysis.

CRISPRi knockdown of PfMT-A70

An enzymatically inactive or 'dead' Cas9 protein (dCas9) was expressed from the pUF-dCas9 plasmid, which is derived from the pUF-Cas9 plasmid backbone described in ref. [54] with the following modifications: the Cas9 was mutated at the RuvC and HNH positions, as described in ref. [57] and the 3×FLAG tag present at the N terminus of the Cas9 protein

in pUF-*Cas9* was removed and a 3xHA tag followed by a *glmS* ribozyme was added to the C terminus of the dCas9 protein in pUF-dCas9 (Supplementary Fig. 2b). Candidate target sites for dCas9 had to be (1) specific, (2) close to the transcription start site, and (3) on the non-template strand and were identified using 'Protospacer'[58].

The guide RNA targeting the PfMT-A70 promoter (gPfMT-A70) (Supplementary Table 12) was synthesized by Eurofins Genomics (Ebersberg, Germany) and cloned into the BtgZ1 restriction site of the pL6-egfp plasmid as described elsewhere[54] using the In-Fusion HD cloning kit (Clontech no. 639649). For the gControl gRNA, the pL6-*egfp* plasmid was unaltered. Cloning and plasmid amplification were performed using XL10-Gold ultracompetent *E. coli* (Agilent Technologies no. 200315) following the manufacturer's protocol and plasmids were purified using the NucleoBond Xtra Maxi Plus kit (Macherey Nagel no. 740416.10) according to the manufacturer's instructions. Ring stage parasites were transfected with 25 μg of pL6 and pUF plasmids by electroporation as described previously[54] and drug-resistant parasites emerged after four weeks of continuous culture in the presence of 2.67 nM WR99210 (Jacobus Pharmaceuticals) and 1.5 μM DSM1. Parasite cloning was performed by limiting dilution as described previously[54].

Quantitative PCR with reverse transcription

Total RNA was extracted from gPfMT-A70 and gControl parasites collected at 12, 24, and 36 h.p.i., as described above. cDNA was generated using the Superscipt VILO cDNA synthesis kit (Thermo Fisher no. 11754050) following the manufacturer's protocol. PfMT-A70 was amplified in technical triplicates using Power Sybr Green PCR Master Mix (Thermo Fisher no. 4367659) and primers PfMT-A70_qPCR-F/PfMT-A70_ qPCR-R (Supplementary Table 12) on a BioRad CFX qPCR machine. A no-RT control (substitution of RT during cDNA synthesis with H_2O) and a no template control (no cDNA added during qPCR amplification) were included in all experiments. Mean starting quantity (SQ-mean) values of technical triplicates were extrapolated from a standard curve made with serial dilutions of genomic DNA. PfMT-A70 levels were normalized to those of an internal housekeeping control gene serine-tRNA ligase (PF3D7_0717700) using primer pair Seryl_qPCR-F/Seryl_qPCR-R (Supplementary Table 7).

dCas9 chromatin immunoprecipitation (dCas9 ChIP)

ChIP experiments were performed for gPfMT-A70 and gControl parasites at 12 h.p.i. at ~2% parasitaemia. RBC cultures (~4% haematocrit) were crosslinked for 10 min by direct addition of methanol-free formaldehyde (1% final concentration) (Thermo Fisher no. 28908). The cross-linking reaction was quenched using a final concentration of 0.125 M glycine for an additional 5 min at room temperature. The iRBC pellet was washed once with DPBS at 4 °C and lysed using 0.15% saponin in DPBS at 4 °C. Parasite cells were collected by centrifugation (3,250*g*, 4 °C, 5 min), washed twice in DPBS at 4 °C, snap frozen in liquid nitrogen, and stored until further use at −80 °C.

For each ChIP experiment, ~2×10^8 parasites were resuspended in 2 ml cytoplasmic lysis buffer (10 mM HEPES pH 8, 10 mM KCl, 0.1 mM EDTA pH 8, plus complete protease inhibitor (PI, Roche no. 11836170001)), transferred to a prechilled 2 ml douncer

homogenizer and set on ice for 30 min. 50 µl 10% IGEPAL CA-630 were added (0.25% final concentration) and parasites were subjected to dounce homogenization. The nuclei were pelleted by centrifugation (10 min, 13,500*g*, 4 °C), and the supernatant (cytoplasmic fraction) was removed. The nuclei pellet was resuspend in 300 µl SDS Lysis buffer (50 mM Tris-HCl pH 8, 10 mM EDTA pH 8, 1% SDS, PI) and transferred to a Diagenode 1.5 ml sonication tube. Chromatin was sonicated to ~ 1,000 bp DNA fragments in a Bioruptor Pico Plus for 24 cycles with 30 s (on/off) intervals at high intensity (12 min total sonication time), and remaining debris were removed by centrifugation (10 min at 13,500*g* at 4 °C). 30 µl of sample were stored as input control at −80 °C. 120 µl of sample were diluted 1:10 in ChIP dilution buffer (16.7 mM Tris-HCl pH 8, 150 mM NaCl, 1.2 mM EDTA pH 8, 1% Triton X-100, 0.01% SDS, PI).

For each sample, 25 µl of protein G magnetic beads (Thermo Fisher no. 10004D) were used and pre-washed three times in 500 µl ChIP dilution buffer. Beads were resuspended in 100 µl ChIP dilution buffer and incubated with 1 µg anti-HA (Abcam no. ab9110) antibody for 2 h with constant rotation at 4 °C. Following antibody binding, beads were washed twice in 1 ml ChIP dilution buffer and resuspended in 25 µl ChIP dilution buffer. The ChIP sample was added to the antibody-conjugated beads and incubated overnight at 4 °C with constant rotation. Following immunoprecipitation, the beads were washed sequentially in 1 ml of low salt wash buffer (20 mM Tris-HCl pH 8, 150 mM NaCl, 2 mM EDTA pH 8, 1% Triton X-100, 0.1% SDS, PI), 1 ml high salt wash buffer (20 mM Tris-HCl pH 8, 500 mM NaCl, 2 mM EDTA pH 8, 1% Triton X-100, 0.1% SDS, PI), one mL LiCl wash buffer (10 mM Tris-HCl pH 8, 250 mM NaCl, 1 mM EDTA pH 8, 0.5% IGEPAL CA-630, 0.5% sodium deoxycholate, PI) and 1 ml TE buffer (10 mM Tris-HCl pH 8, 1 mM EDTA pH 8). For each wash, the beads were rotated for 5 min at 4 °C except for the last TE wash, which was performed at room temperature. The beads were subsequently resuspended in 210 µl elution buffer (50 mM Tris-HCl pH 8, 10 mM EDTA pH 8, 1% SDS) and protein-DNA complexes were eluted by 30 min incubation at 65 °C in an agitator (900 rpm 1 min, still 30 s). At this step, the input sample was recovered from storage, diluted with 170 µl elution buffer, and processed in parallel with the IP sample.

Protein-DNA complexes were reverse crosslinked by incubation at 65 °C for 6 h. Samples were diluted with 200 µl of TE buffer and incubated with RNaseA (0.2 mg ml^{-1} final concentration) (Thermo Fisher no. EN0531) at 37 °C for 2 h. Proteinase K (0.2 µg ml^{-1} final concentration) (NEB no. P8107S) was then added and samples were incubated at 55 °C for 2 h. DNA was purified by adding 400 µl phenol:chloroform:isoamyl alcohol, and phases were separated by centrifugation (10 min, 13,500*g*, 4 °C) after vigorous vortexing. 16 µl of 5 M NaCl (200 mM final concentration) and 30 µg glycogen were added to the aqueous phase, and DNA was precipitated by adding 800 µl 100% EtOH 4 °C and incubating for 30 min at −20 °C. DNA was pelleted by centrifugation (20,000*g*, 10 min, 4 °C) and washed with 500 µl 80% EtOH 4 °C. After centrifugation, the DNA pellet was air-dried and resuspended in 30 µl of 10 mM Tris-HCl pH 8.0.

m^{6}A immunoprecipitation and sequencing

Two replicates were sampled for both cell lines expressing dCas9 and either a non-targeting control gRNA (gControl) or the PfMT-A70 promoter-targeting gRNA (gPfMT-A70). Total RNA from highly synchronous parasites was collected at 12, 24 and 36 h.p.i. as described above, followed by poly(A) RNA enrichment using the Dynabeads mRNA purification kit (Thermo Fisher no. 61006).

300–500 ng purified mRNA was fragmented for 15 min at 70 °C to ~ 100 nt using the NEBNext fragmentation module (NEB no. E6150S) and purified using the Qiagen MinElute kit (Qiagen no. 74204) with slight modifications: to also purify small RNA <200 nt, 100 µl of RNA sample was supplemented with 350 µl of lysis buffer (provided in the kit) followed by the addition of 700 µl of 100% ethanol. 20 ng fragmented mRNA were stored as input sample at −80 °C.

For each m^{6}A-IP, 25 µl of protein A/G magnetic beads (Thermo Fisher no. 88802) were diluted in 250 µl reaction buffer (150 mM NaCl, 10 mM Tris-HCl pH 7.5, 0.1% IGEPAL CA-630 in nuclease-free H_2O) and washed twice in 250 µl reaction buffer. The beads were resuspended in 100 µl reaction buffer and incubated with 2.5 µg anti-m^{6}A antibody (Abcam no. ab151230) for 30 min at room temperature with constant rotation. The beads were subsequently washed three times with 0.5 ml reaction buffer. For each m^{6}A-IP, 300–500 ng fragmented mRNA were diluted with nuclease-free H_2O to a final volume of 395 µl, supplemented with 5 µl RNase inhibitor (Promega no. N2615), 100 µl 5× reaction buffer (750 mM NaCl, 50 mM Tris-HCl pH 7.5, 0.5% IGEPAL CA-630 in nuclease-free H_2O) and added to the antibody-bead mixture. The sample was incubated at 4 °C with constant rotation for 2 h. Following immunoprecipitation, the supernatant was removed and the beads were washed twice in 250 µl reaction buffer, twice in 250 µl low salt wash buffer (50 mM NaCl, 10 mM Tris-HCl pH 7.5, 0.1% IGEPAL CA-630 in nuclease-free H_2O), and twice in 250 µl high salt wash buffer (500 mM NaCl, 10 mM Tris-HCl pH 7.5, 0.1% IGEPAL CA-630 in nuclease-free H_2O), all at 4 °C. m^{6}A mRNA fragments were competitively eluted by two successive incubations (1 h, 1,000 rpm continuous shaking at 4 °C) with 100 µl elution buffer (6.7 mM m^{6}A 5-monophosphate sodium salt (Sigma no. M2780-10MG), 150 mM NaCl, 10 mM Tris-HCl pH 7.5, 0.1%, 400 U RNase inhibitor (Promega no. N2615) in nuclease-free H_2O). RNA was purified using the Qiagen MinElute kit (Qiagen no. 74204) as described above.

RNA sequencing libraries were prepared using the Illumina TruSeq stranded RNA Library Prep Kit (Illumina no. RS-122-2101) according to the manufacturer's instructions with slight modifications. To account for the AT-richness of cDNA fragments, we used the KAPA Hifi polymerase (Roche no. 07958846001) at the library amplification step. The libraries were sequenced on an Illumina NextSeq 500 platform with a 1 × 150 bp single-end read layout.

RNA-sequencing for differential gene expression analysis

For RNA sequencing, three replicates of highly synchronous gPfMT-A70 and two replicates of gControl parasites were collected at 12, 24 and 36 h.p.i. Total RNA was extracted as

described above and poly(A) RNA was enriched using the Dynabeads mRNA purification kit (Thermo Fisher no. 61006).

RNA sequencing libraries were prepared using the Illumina TruSeq stranded RNA Library Prep Kit (Illumina no. RS-122-2101) according to the manufacturer's instructions with slight modifications. To account for the AT-richness of cDNA fragments, we used the KAPA Hifi polymerase (Roche no. 07958846001) at the library amplification step. The libraries were sequenced on an Illumina NextSeq 500 platform with a 1 × 150 bp single-end read layout.

Phylogenetic analysis of the m^{6}A writer and reader complex

Candidate proteins of the *P. falciparum* m^{6}A writer complex were identified by searching known members of the m^{6}A writer complex from other eukaryotes against the *P. falciparum* proteome using blastp[59]. Protein alignments were generated using mafft[60] and visualized in Geneious[61]. For the phylogenetic analysis, gaps in the protein alignments were removed with trimal[62] and the best phylogenetic model was calculated using protTest3[63]. Phylogenetic trees were constructed using MEGA (v7)[64] with 1,000 bootstrap replicates, and the bootstrap consensus trees were visualized in FigTree (v1.4.3, http://tree.bio.ed.ac.uk/software/figtree/). Low-complexity disorder regions were annotated using D2P2[65]

Identification and quantification of mRNA modifications by LC-MS/MS

LC/MS data was extracted using the MassHunter Qualitative and Quantitative Analysis Software (version B06.00) and further analysed as follows. Briefly, to account for any background signal that could be a contribution from the salts and enzymes in the digestion buffer, the signal intensity (that is area under the curve) for each ribonucleoside is first subtracted from a matrix sample (without any RNA). To calculate relative levels of each modified ribonucleoside and to adjust for different injection amounts of RNA in each sample, the matrix-corrected intensity of the modified ribonucleosides (for example m^{6}A) was then divided by the intensity of the respective canonical ribonucleoside (for example rA). To adjust day-to-day fluctuation in retention time of the mass spectrometer, an internal standard ([^{15}N]-2'-deoxyadenosine) was spiked into each sample during RNA digestion. The absolute values for N^6-methyladenosine (Fig. 1e) were calculated by using an external calibration curve prepared using known standards to account for the difference in ionization efficiency in the mass spectrometer (Supplementary Table 2).

For visualization of lifecycle-dependent changes in the quantities of modified ribonucleosides (Fig. 1b), the modified nucleotide ratios (for example m$^{\lambda}$/A) were scaled to row *Z*-sores following the formula z = (x-u)/s, with x = actual measured value; u = average over all samples and s = standard deviation over all samples.

dCas9 ChIP sequencing and analysis

DNA sequencing libraries were prepared using the Diagenode MicroPlex Library Preparation kit (Diagenode no. C05010014) according to the manufacturer's instructions and sequenced on an Illumina NextSeq 500 platform with a 1 × 150 bp single-end read layout. Raw image files were converted to fastq sequence files using Illumina's bcl2fastq (v2.19).

Reads were aligned to the *P. falciparum* genome (plasmoDB.org, v3, release v28)[28,66] using bwa 'mem'[67] allowing only unique read mappings (option '-c 1'). Optical duplicates and alignments with a quality score <20 were removed using samtools' 'rmdup' and 'view'[68], respectively.

For coverage plots of gPfMT-A70 and gControl (Fig. 3b) ChIP-seq experiments, deeptool's bamCompare[69] was used to normalize the read coverage per genome position (option '–bs 1') in the respective input and ChIP samples to the total number of mapped reads in each library (option '– normalizeUsingRPKM'). Normalized input coverage per bin was subtracted from the ChIP values (option '–ratio subtract') and coverage plots were visualized in plasmoDB's build-in genome browser together with other chromatin features (plasmoDB.org).

For genome-wide coverage plots (Fig. 3c), the same approach was used as above, but genome coverage was calculated not per genome position but for 1000 nt windows. To further remove background levels of unspecific dCas9 binding, the gControl ChIP-input coverage was subtracted from the gPfMT-A70 ChIP-input coverage and visualized using circos[70].

RNA sequencing read mapping

Raw image files were converted to fastq sequence files using Illumina's bcl2fastq (v2.19). The reads were aligned to the *P. falciparum* genome (plasmoDB.org, v3, release 28)[28] using bwa 'mem'[67] allowing only unique read mappings (option '-c 1'). Optical duplicates and alignments with a quality score <20 were removed using samtools' 'rmdup' and 'view'[68], respectively.

m^{6}A peak calling

At each time point, we separately identified significant (FDR ≤0.05) m^{6}A peaks for each replicate (that is, 2× gControl and 2× gPfMT-A70) using macs2[71] with default settings but without prior peak modelling (option '– nomodel'), the fragment size set to 150 bp (option '–extsize 150') and the genome size (option -g) set to 11×10^6. To generate a single robust set of m^{6}A peaks for each time point, we identified overlapping m^{6}A peaks using bedtools 'multiinter'[72] and only retained those that were present in ≥two of the four samples at each time point. Overlaps of m^{6}A peaks and genic regions were identified using bedtools 'intersect'[72].

m^{6}A motif identification

For the m^{6}A motif analysis, sequences ±100 bp of the m^{6}A peak summit were extracted from the *P. falciparum* genome using bedtools 'getfasta'[72], taking the strandedness of the underlying transcript into account (option '-s'). A random set of control sequences was constructed as following. For each m^{6}A peak in a transcript, a random position in the same transcript was calculated using bash 'shuffle' implemented in a custom script. Sequences ±100 bp surrounding the random site were extracted using bedtools 'getfasta' as described above. Significantly enriched motifs in the m^{6}A peak region were subsequently identified with homer2 'findMotif.pl'[73].

5-mers in the m^{6}A peak region and controls sequence set were counted using jellyfish[74]. The deduced sequence motif was generated using all 5-mers with an AC context that were enriched ≥two-fold in the m^{6}A peak region compared to the random control using weblogo[75], taking their frequency in the m^{6}A peak region into account. The central enrichment of the deduced sequence motif was calculated using homer2 'annotatePeaks.pl'.

m^{6}A enrichment calculation

m^{6}A enrichments were calculated following the approach originally reported[39,76]. Briefly, for each time point, the number of reads mapping to an m^{6}A peak in the m^{6}A-IP and m^{6}A-input sample was calculated using bedtools 'coverage-count' and normalized to the total number of mapped reads in each sample. m^{6}A enrichments were then calculated as m^{6}A-IP/input for each peak and in each individual sample. To calculate decreases in global m^{6}A enrichment in gPfMT-A70 (Fig. 5b, top) at each time point, m^{6}A enrichments of every peak were averaged over the two replicates of each condition. Of note, m^{6}A enrichments were highly reproducible (Fig. 5b, bottom) and the individual m^{6}A enrichment values of each m^{6}A peak and replicate are shown in Supplementary Tables 4–6).

For visualization of changes in m^{6}A enrichments (Fig. 5a), we used cgat's 'bam2geneprofile'[77]. Briefly, the read coverage from m^{6}A-IP and m^{6}A-input libraries of each sample was calculated and normalized to the total size of mapped reads in each library in 10 nt windows and in a region ±2 kb surrounding the m^{6}A peak summit. m^{6}A enrichments in each 10 nt window were calculated as the ration of m^{6}A-IP over m^{6}A-input.

Differential gene expression analysis

RNA sequencing reads for three replicates of the gPfMT-A70 and two replicates of the gControl cell lines were mapped to the *P. falciparum* genome and quality filtered as described above. Strand specific gene counts were calculated using htseq-count[78].

Differential gene expression analysis was performed using DESeq2[79] using all replicates of gPfMT-A70 and gControl at each time point. Due to their monoallelic nature, genes encoding variant surface antigens (*var*, *rifin* and *stevor*) were excluded from the analysis. MA plots were generated using the 'baseMean' (mean normalized read count over all replicates and conditions) and 'log$_2$FoldChange' values (gPfMT-A70 over gControl) as determined by DESeq2 for each time point.

For the comparison of transcript abundances (Fig. 5c, left), we first averaged the m^{6}A enrichment of every m^{6}A peak over the two replicates of each condition as described above. We then retained only those m^{6}A-methylated transcripts that harbour m^{6}A peaks with the most pronounced decreases in m^{6}A enrichment (that is, ≥two-fold decrease). For the direct comparison of transcript log$_2$ fold changes (Fig. 5c, right), the set of transcripts with reduced m^{6}A enrichments was compared to non-methylated transcripts being expressed in the same range of mean normalized read counts (that is, baseMean value).

RPKM (reads per kilobase per exon per one million mapped reads) values were calculated in R using the command rpkm() from the package edgeR[80].

mRNA stability and translational efficiency analysis

For the comparative analysis of m^6A methylation and mRNA stability or translation efficiency, we used m^6A-methylated transcripts that were expressed in the top 50% of all transcripts at a given time point as calculated by RNA-seq of the m^6A-input samples and with a peak density of ≥ 0.2 m^6A peaks per kilobase of exon. Corresponding mRNA stability (measured as mRNA half-life) and translational efficiency values of the same parasite developmental stages were extracted from refs. [13,15], respectively. Independent measurements of mRNA stability data were retrieved from ref. [10].

Statistical analysis

All statistical analysis were performed in R[81]. To test for a normal distribution of the data, the Shapiro–Wilk normality test was used. To test for significance between two groups, a two-sided independent-samples *t*-test or two-sided Mann-Whitney *U*-test were performed as indicated. Gene Ontology enrichments were calculated using the build-in tool at plasmoDB.org. Correlations between replicates were calculated in R using function cor() with default settings (calculation of Pearson correlation coefficient *r*).

All heatmaps were visualized using the function heatmap2() in the R gplots package with row *z*-score normalization. *Z*-scores were calculated over all samples ('rows') following the formula $z = (x-u)/s$, with x = given value of a specific sample; u = average over all samples and s = standard deviation over all samples.

Supplementary Material

Refer to Web version on PubMed Central for supplementary material.

Acknowledgements

We thank A. Claës, C. Scheidig-Benatar and P. Chen for help with parasite culture. Protein mass-spectrometry was performed at the Biopolymers and Proteomics core of The Koch Institute Swanson Biotechnology Center. This work was supported by a European Research Council Advanced Grant (PlasmoSilencing 670301) and the French Parasitology consortium ParaFrap (ANR-11-LABX0024) to A.Scherf. Work in the labs of P.R.P. and P.C.D. was funded by the National Research Foundation Singapore under its Singapore-MIT Alliance for Research and Technology (SMART) Centre, Infectious Disease and Antimicrobial Resistance IRGs. S.B. and J.M.B. were supported by an EMBO fellowship (S.B.: ALTF 1444-2016; J.M.B.: ALTF 180-2015). A.Si. acknowledges financial support from the Singapore-MIT Alliance (SMA) Graduate Fellowships.

Data availability

All sequencing data are accessible on the Gene Expression Omnibus database (https://www.ncbi.nlm.nih.gov/geo) under study accession number GSE123839. Raw sequence data are accessible on the NCBI Sequence Read Archive (SRA) under BioProject accession number PRJNA473770. Proteomics and mRNA modification LC-MS/MS data are deposited at the Chorus database with accession number 1579.

References

1. World Malaria Report 2018. World Health Organization; 2018.

2. Bozdech Z, et al. The transcriptome of the intraerythrocytic developmental cycle of *Plasmodium falciparum* . PLoS Biol. 2003; 1 :85–100.
3. Scherf A, Lopez-Rubio JJ, Riviere L. Antigenic variation in *Plasmodium falciparum* . Annu Rev Microbiol. 2008; 62 :445–470. [PubMed: 18785843]
4. Kafsack BFC, et al. A transcriptional switch underlies commitment to sexual development in malaria parasites. Nature. 2014; 507 :248–252. [PubMed: 24572369]
5. Salcedo-Amaya AM, et al. Dynamic histone H3 epigenome marking during the intraerythrocytic cycle of *Plasmodium falciparum* . Proc Natl Acad Sci USA. 2009; 106 :9655–9660. [PubMed: 19497874]
6. Kensche PR, et al. The nucleosome landscape of *Plasmodium falciparum*>reveals chromatin architecture and dynamics of regulatory sequences. Nucleic Acids Res. 2016; 44 :2110–2124. [PubMed: 26578577]
7. Toenhake CG, et al. Chromatin accessibility-based characterization of the gene regulatory network underlying *lasmodium falciparum* blood-stage development. Cell Host Microbe. 2018; 23 :557–569. [PubMed: 29649445]
8. Ganesan K, et al. A genetically hard-wired metabolic transcriptome in *Plasmodium falciparum* fails to mount protective responses to lethal antifolates. PLoS Pathog. 2008; 4 e1000214 [PubMed: 19023412]
9. Llinás M, Bozdech Z, Wong ED, Adai AT, DeRisi JL. Comparative whole genome transcriptome analysis of three *Plasmodium falciparum* strains. Nucleic Acids Res. 2006; 34 :1166–1173. [PubMed: 16493140]
10. Painter HJ, et al. Genome-wide real-time in vivo transcriptional dynamics during *Plasmodium falciparum* blood-stage development. Nat Commun. 2018; 9 2656 [PubMed: 29985403]
11. Hughes KR, Philip N, Starnes GL, Taylor S, Waters AP. From cradle to grave: RNA biology in malaria parasites. WIRES RNA. 2010; 1 :287–303. [PubMed: 21935891]
12. Vembar SS, Droll D, Scherf A. Translational regulation in blood stages of the malaria parasite *Plasmodium* spp.: systems-wide studies pave the way. WIRES RNA. 2016; 7 :772–792. [PubMed: 27230797]
13. Shock JL, Fischer KF, DeRisi JL. Whole-genome analysis of mRNA decay in *Plasmodium falciparum* reveals a global lengthening of mRNA half-life during the intra-erythrocytic development cycle. Genome Biol. 2007; 8 R134 [PubMed: 17612404]
14. Foth BJ, Zhang N, Mok S, Preiser PR, Bozdech Z. Quantitative protein expression profiling reveals extensive post-transcriptional regulation and post-translational modifications in schizont-stage malaria parasites. Genome Biol. 2008; 9 R177 [PubMed: 19091060]
15. Caro F, Ahyong V, Betegon M, DeRisi JL. Genome-wide regulatory dynamics of translation in the *Plasmodium falciparum* asexual blood stages. eLife. 2014; 3 e04106
16. Roundtree IA, Evans ME, Pan T, He C. Dynamic RNA modifications in gene expression regulation. Cell. 2017; 169 :1187–1200. [PubMed: 28622506]
17. Meyer KD, Jaffrey SR. Rethinking m^6A readers, writers, and erasers. Annu Rev Cell Dev Biol. 2017; 33 :319–342. [PubMed: 28759256]
18. Śledź P, Jinek M. Structural insights into the molecular mechanism of the m(6)A writer complex. eLife. 2016; 5 e18434 [PubMed: 27627798]
19. Wang Y, et al. N6-methyladenosine modification destabilizes developmental regulators in embryonic stem cells. Nat Cell Biol. 2014; 16 :191–198. [PubMed: 24394384]
20. Ping X-L, et al. Mammalian WTAP is a regulatory subunit of the RNA N6-methyladenosine methyltransferase. Cell Res. 2014; 24 :177–189. [PubMed: 24407421]
21. Liu N, et al. N(6)-methyladenosine-dependent RNA structural switches regulate RNA-protein interactions. Nature. 2015; 518 :560–564. [PubMed: 25719671]
22. Meyer KD, et al. 5’ UTR m(6)A promotes cap-independent translation. Cell. 2015; 163 :999–1010. [PubMed: 26593424]
23. Wang X, et al. N6-methyladenosine-dependent regulation of messenger RNA stability. Nature. 2014; 505 :117–120. [PubMed: 24284625]

24. Patil DP, Pickering BF, Jaffrey SR. Reading m^{6}A in the transcriptome: m^{6}A-binding proteins. Trends Cell Biol. 2018; 28 :113–127. [PubMed: 29103884]
25. Vu LP, et al. The N6-methyladenosine (m6A)-forming enzyme METTL3 controls myeloid differentiation of normal hematopoietic and leukemia cells. Nat Med. 2017; 23 :1369–1376. [PubMed: 28920958]
26. Lence T, et al. m6A modulates neuronal functions and sex determination in *Drosophila* . Nature. 2016; 540 :242–247. [PubMed: 27919077]
27. Schwartz S, et al. High-resolution mapping reveals a conserved, widespread, dynamic mRNA methylation program in yeast meiosis. Cell. 2013; 155 :1409–1421. [PubMed: 24269006]
28. Gardner MJ, et al. Genome sequence of the human malaria parasite *Plasmodium falciparum* . Nature. 2002; 419 :498–511. [PubMed: 12368864]
29. Larson MH, et al. CRISPR interference (CRISPRi) for sequence-specific control of gene expression. Nat Protoc. 2013; 8 :2180–2196. [PubMed: 24136345]
30. Xiao B, et al. Epigenetic editing by CRISPR/dCas9 in *Plasmodium falciparum* . Proc Natl Acad Sci USA. 2019; 116 :255–260. [PubMed: 30584102]
31. Fujita T, Fujii H. Efficient isolation of specific genomic regions and identification of associated proteins by engineered DNA-binding molecule-mediated chromatin immunoprecipitation (enChIP) using CRISPR. Biochem Biophys Res Commun. 2013; 439 :132–136. [PubMed: 23942116]
32. Ponts N, et al. Nucleosome landscape and control of transcription in the human malaria parasite. Genome Res. 2010; 20 :228–238. [PubMed: 20054063]
33. Bártfai R, et al. H2A.Z demarcates intergenic regions of the *Plasmodium falciparum* epigenome that are dynamically marked by H3K9ac and H3K4me3. PLoS Pathog. 2010; 6 e1001223 [PubMed: 21187892]
34. Adjalley SH, Chabbert CD, Klaus B, Pelechano V, Steinmetz LM. Landscape and dynamics of transcription Initiation in the malaria parasite *Plasmodium falciparum* . Cell Rep. 2016; 14 :2463–2475. [PubMed: 26947071]
35. Linder B, et al. Single-nucleotide-resolution mapping of m6A and m6Am throughout the transcriptome. Nat Methods. 2015; 12 :767–772. [PubMed: 26121403]
36. Stevens AT, Howe DK, Hunt AG. Characterization of mRNA polyadenylation in the apicomplexa. PLoS One. 2018; 13 e0203317 [PubMed: 30161237]
37. Engel M, et al. The role of m6A/m-RNA methylation in stress response regulation. Neuron. 2018; 99 :389–403. [PubMed: 30048615]
38. Iyer LM, Zhang D, Aravind L. Adenine methylation in eukaryotes: apprehending the complex evolutionary history and functional potential of an epigenetic modification. Bioessays. 2016; 38 :27–40. [PubMed: 26660621]
39. Schwartz S, et al. Perturbation of m6A writers reveals two distinct classes of mRNA methylation at internal and 5’ sites. Cell Rep. 2014; 8 :284–296. [PubMed: 24981863]
40. Wen J, et al. Zc3h13 regulates nuclear RNA m6A methylation and mouse embryonic stem cell self-renewal. Mol Cell. 2018; 69 :1028–1038. [PubMed: 29547716]
41. Růžička K, et al. Identification of factors required for m6A mRNA methylation in *Arabidopsis* reveals a role for the conserved E3 ubiquitin ligase HAKAI. New Phytol. 2017; 215 :157–172. [PubMed: 28503769]
42. Oehring SC, et al. Organellar proteomics reveals hundreds of novel nuclear proteins in the malaria parasite *Plasmodium falciparum* . Genome Biol. 2012; 13 R108 [PubMed: 23181666]
43. Yue Y, et al. VIRMA mediates preferential m6A mRNA methylation in 3’UTR and near stop codon and associates with alternative polyadenylation. Cell Disco. 2018; 4 :10.
44. Garcia-Campos MA, et al. Deciphering the ‘m6A code’ via quantitative profiling of m6A at single-nucleotide resolution. 2019; doi: 10.1101/571679
45. Ke S, et al. m6A mRNA modifications are deposited in nascent pre-mRNA and are not required for splicing but do specify cytoplasmic turnover. Genes Dev. 2017; 31 :990–1006. [PubMed: 28637692]
46. Patil DP, et al. M6A RNA methylation promotes XIST-mediated transcriptional repression. Nature. 2016; 537 :369–373. [PubMed: 27602518]

47. Lasonder E, et al. Integrated transcriptomic and proteomic analyses of P. falciparum gametocytes: molecular insight into sex-specific processes and translational repression. Nucleic Acids Res. 2016; 44 :6087–6101. [PubMed: 27298255]
48. Lindner SE, et al. Extensive transcriptional and translational regulation occur during the maturation of malaria parasite sporozoites. 2019; doi: 10.1101/642298
49. Cui L, Lindner S, Miao J. Translational regulation during stage transitions in malaria parasites. Ann New York Acad Sci. 2015; 1342 :1–9. [PubMed: 25387887]
50. Lopez-Rubio JJ, Mancio-Silva L, Scherf A. Genome-wide analysis of heterochromatin associates clonally variant gene regulation with perinuclear repressive centers in malaria parasites. Cell Host Microbe. 2009; 5 :179–190. [PubMed: 19218088]
51. Vembar SS, Macpherson CR, Sismeiro O, Coppée J-Y, Scherf A. The PfAlba1 RNA-binding protein is an important regulator of translational timing in *Plasmodium falciparum* blood stages. Genome Biol. 2015; 16 :212. [PubMed: 26415947]
52. Ng CS, et al. tRNA epitranscriptomics and biased codon are linked to proteome expression in *Plasmodium falciparum* . Mol Syst Biol. 2018; 14 e8009 [PubMed: 30287681]
53. Crabb BS, et al. Transfection of the human malaria parasite *Plasmodium falciparum* . Methods Mol Biol. 2004; 270 :263–276. [PubMed: 15153633]
54. Ghorbal M, et al. Genome editing in the human malaria parasite *Plasmodium falciparum* using the CRISPR-Cas9 system. Nat Biotechnol. 2014; 32 :819–821. [PubMed: 24880488]
55. Mesén-Ramírez P, et al. Stable translocation intermediates jam global protein export in *Plasmodium falciparum* parasites and link the PTEX component EXP2 with translocation activity. PLoS Pathog. 2016; 12 e1005618 [PubMed: 27168322]
56. Perkins DN, Pappin DJ, Creasy DM, Cottrell JS. Probability-based protein identification by searching sequence databases using mass spectrometry data. Electrophoresis. 1999; 20 :3551–3567. [PubMed: 10612281]
57. Qi LS, et al. Repurposing CRISPR as an RNA-guided platform for sequence-specific control of gene expression. Cell. 2013; 152 :1173–1183. [PubMed: 23452860]
58. MacPherson CR, Scherf A. Flexible guide-RNA design for CRISPR applications using Protospacer Workbench. Nat Biotechnol. 2015; 33 :805–806. [PubMed: 26121414]
59. Altschul SF, Gish W, Miller W, Myers EW, Lipman DJ. Basic local alignment search tool. J Mol Biol. 1990; 215 :403–410. [PubMed: 2231712]
60. Katoh K, Standley DM. MAFFT multiple sequence alignment software version 7: improvements in performance and usability. Mol Biol Evol. 2013; 30 :772–780. [PubMed: 23329690]
61. Kearse M, et al. Geneious Basic: an integrated and extendable desktop software platform for the organization and analysis of sequence data. Bioinformatics. 2012; 28 :1647–1649. [PubMed: 22543367]
62. Capella-Gutierrez S, Silla-Martinez JM, Gabaldon T. trimAl: a tool for automated alignment trimming in large-scale phylogenetic analyses. Bioinformatics. 2009; 25 :1972–1973. [PubMed: 19505945]
63. Darriba D, Taboada GL, Doallo R, Posada D. ProtTest 3: fast selection of best-fit models of protein evolution. Bioinformatics. 2011; 27 :1164–1165. [PubMed: 21335321]
64. Kumar S, Stecher G, Tamura K. MEGA7: molecular evolutionary genetics analysis version 7.0 for bigger datasets. Mol Biol Evol. 2016; 33 :1870–1874. [PubMed: 27004904]
65. Oates ME, et al. D^2P^2: database of disordered protein predictions. Nucleic Acids Res. 2013; 41 :D508–D516. [PubMed: 23203878]
66. Aurrecoechea C, et al. EuPathDB: the eukaryotic pathogen genomics database resource. Nucleic Acids Res. 2017; 45 :D581–D591. [PubMed: 27903906]
67. Li H, Durbin R. Fast and accurate short read alignment with BurrowsWheeler transform. Bioinformatics. 2009; 25 :1754–1760. [PubMed: 19451168]
68. Li H, et al. The sequence alignment/map format and SAMtools. Bioinformatics. 2009; 25 :2078–2079. [PubMed: 19505943]
69. Ramírez F, et al. deepTools2: a next generation web server for deepsequencing data analysis. Nucleic Acids Res. 2016; 44 :W160–W165. [PubMed: 27079975]

70. Krzywinski M, et al. Circos: an information aesthetic for comparative genomics. Genome Res. 2009; 19 :1639–1645. [PubMed: 19541911]
71. Zhang Y, et al. Model-based analysis of ChIP-Seq (MACS). Genome Biol. 2008; 9 R137 [PubMed: 18798982]
72. Quinlan AR, Hall IM. BEDTools: a flexible suite of utilities for comparing genomic features. Bioinformatics. 2010; 26 :841–842. [PubMed: 20110278]
73. Heinz S, et al. Simple combinations of lineage-determining transcription factors prime cis-regulatory elements required for macrophage and B cell identities. Mol Cell. 2010; 38 :576–589. [PubMed: 20513432]
74. Marçais G, Kingsford C. A fast, lock-free approach for efficient parallel counting of occurrences of k-mers. Bioinformatics. 2011; 27 :764–770. [PubMed: 21217122]
75. Crooks GE, Hon G, Chandonia J-M, Brenner SE. WebLogo: a sequence logo generator. Genome Res. 2004; 14 :1188–1190. [PubMed: 15173120]
76. Meyer KD, et al. Comprehensive analysis of mRNA methylation reveals enrichment in 3′ UTRs and near stop codons. Cell. 2012; 149 :1635–1646. [PubMed: 22608085]
77. Sims D, et al. CGAT: computational genomics analysis toolkit. Bioinformatics. 2014; 30 :1290–1291. [PubMed: 24395753]
78. Anders S, Pyl PT, Huber W. HTSeq–a Python framework to work with high-throughput sequencing data. Bioinformatics. 2015; 31 :166–169. [PubMed: 25260700]
79. Love MI, Huber W, Anders S. Moderated estimation of fold change and dispersion for RNA-seq data with DESeq2. Genome Biol. 2014; 15 :550. [PubMed: 25516281]
80. Robinson MD, McCarthy DJ, Smyth GK. edgeR: a bioconductor package for differential expression analysis of digital gene expression data. Bioinformatics. 2010; 26 :139–140. [PubMed: 19910308]
81. R: A language and environment for statistical computing. R Development Core Team; 2012.
82. Broadbent KM, et al. Strand-specific RNA sequencing in *Plasmodium falciparum* malaria identifies developmentally regulated long non-coding RNA and circular RNA. BMC Genom. 2015; 16 :454.

Europe PMC Funders Author Manuscripts

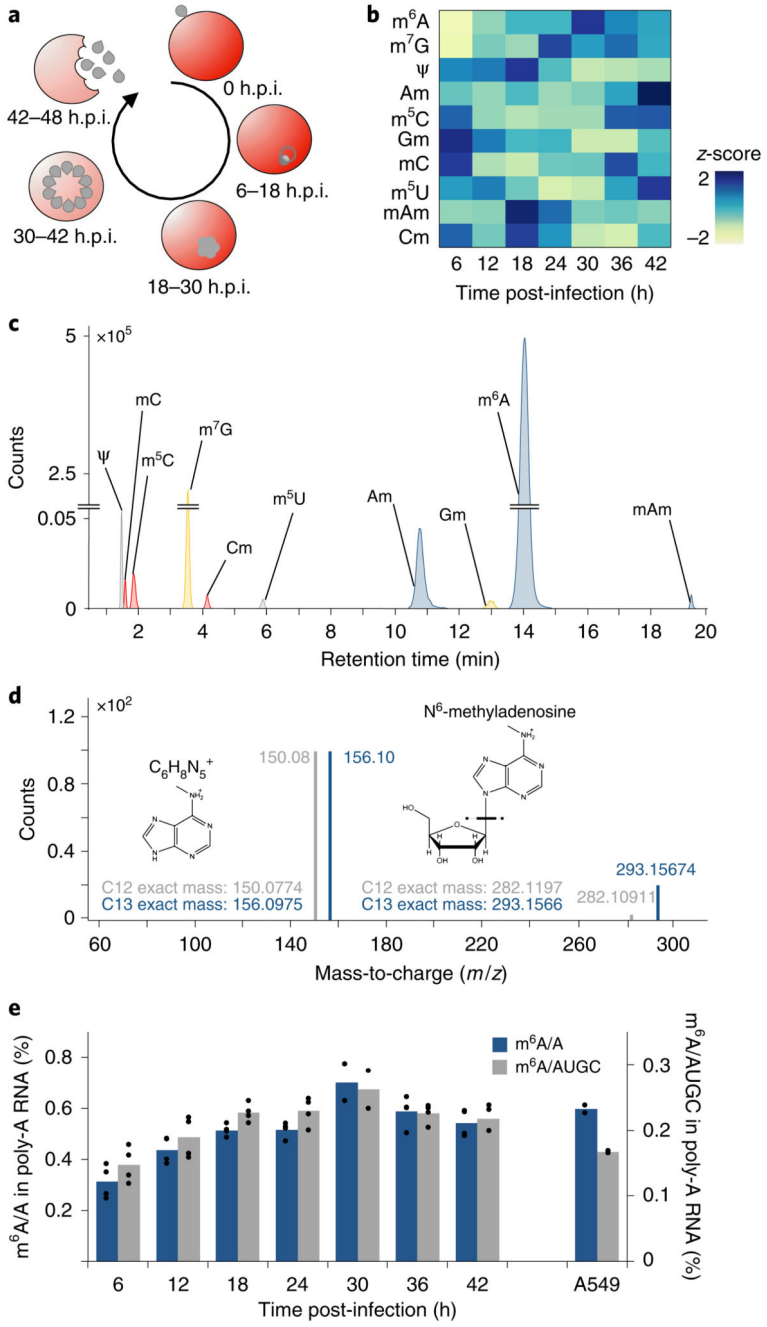

Fig. 1. global dynamics of mRNA modifications during the *P. falciparum* iDC.

a, Diagram illustrating the asexual replicative cycle of *P. falciparum* inside human RBCs including RBC invasion, host cell remodelling, replication via schizogony and RBC egress. **b**, Heatmap of normalized abundances (modification/canonical nucleotide) of ten mRNA modifications measured by LC-MS/MS at 6-h intervals over the course of the IDC (see also Supplementary Fig. 1d). Average of four biological replicates for each modification and timepoint, except 30 h.p.i. ($n = 2$). Blue indicates a high z-score while yellow indicates a low z-score (see Methods). **c**, LC-MS/MS extracted ion chromatograms of modified nucleotides

analysed in parasite mRNA collected at 36 h.p.i. rC, cytosine; rU, uracil; rG, guanosine; rA, adenosine; m^6A, N^6-methyladenosine; m^7G, N^7-methyl-2'-guanosine; Ψ, pseudouridine; Am, 2'-O-methyladenosine; m^5C, 5-methylcytosine; Gm, 2'-O-methylguanosine; mC, (3 or 4)-methylcytosine; m^5U, 5-methyluridine; mAm, *-methyl-2'-O-methyladenosine; Cm, 2'-O-methylcytosine. **d**, Analysis of m^6A by high-resolution mass spectrometry. Product ion spectrum of m^6A in *P. falciparum* mRNA (grey) using heavy (C13) labelled *E. coli* tRNA (blue) as a standard. Fragmentation of *m*/*z* 282.12 (C12-red) and *m*/*z* 293.16 (C13-blue) leads to the breakage of the glycosidic bond resulting in the loss of the ribose sugar (132 Da) to form a daughter ion having a *m*/*z* 150.08 (C12-red) and *m*/*z* 156.10 (C13-blue). **e**, Global dynamics of calibrated m^6A/A (blue) and m^6A/AUGC (grey) levels across the asexual replicative cycle in 6-h intervals. As a reference, human A549 mRNA was analysed in parallel[39]. *n* = 4 for all time points except 30 h.p.i. (*n* = 2); *n* = 2 for human A549 samples. Points represent individual biological replicates with bars showing the mean.

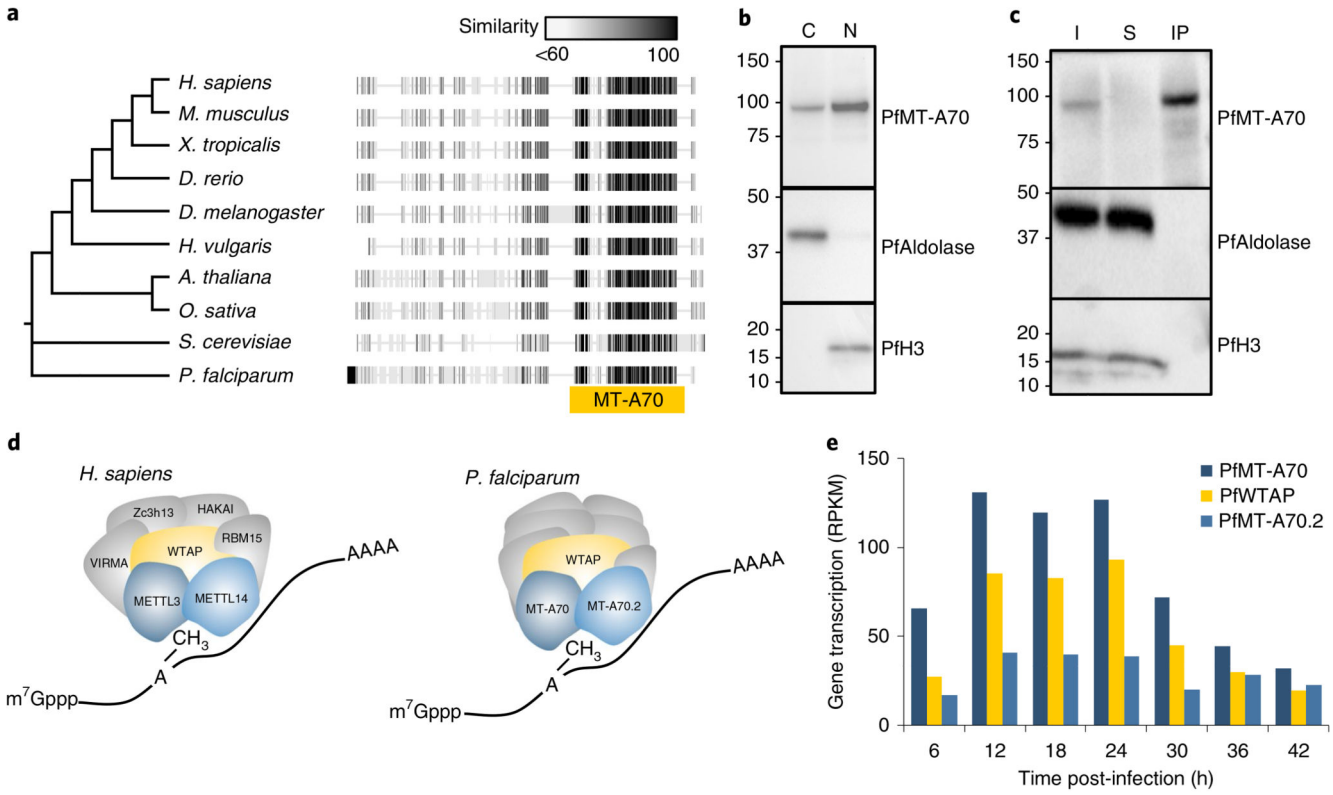

Fig. 2. Characterization of the *P. falciparum* m^{6}A writer complex.

a, Phylogenetic tree and protein alignments of PfMT-A70 with orthologues in other eukaryotes. The location of the MT-A70 domain is shown below the alignment (yellow bar). The grey-scale gradient indicates the percentage similarity across all proteins at an aligned position. **b**, Western blot analysis showing the enrichment of HA-tagged PfMT-A70 in the cytoplasmic (C) and nuclear (N) cell fractions at 12 h.p.i. PfAldolase and histone H3 serve as controls for the cytoplasmic and nuclear fraction, respectively. Numbers on the left indicate molecular weight in kilodaltons. Data are representative of three independent biological experiments. **c**, Western blot analysis of PfMT-A70-HA co-IP with anti-HA antibodies. PfAldolase and histone H3 demonstrate efficacy of the anti-HA co-IP. Numbers on the left indicate molecular weight in kilodaltons. I, input; S, supernatant; IP, co-IP fraction. Data are representative of three independent biological experiments. **d**, Schematic of the human m^{6}A writer complex (left) and the *P. falciparum* proteins that were co-immunoprecipitated with PfMT-A70. Orthologous proteins are highlighted in the same colour; that is, METTL3/PfMT-A70, METTL14/PfMT-A70.2 and WTAP/PfWTAP. Co-factors of the human core m^{6}A writer complex (left) and putative, non-conserved co-factors of *P. falciparum* (right) are shown in grey. **e**, Gene transcription (in reads per kilobase of exon per one million mapped reads (RPKM))[82] of putative orthologues of the *P. falciparum* m^{6}A writer complex at 6-h intervals over the course of the IDC.

Europe PMC Funders Author Manuscripts

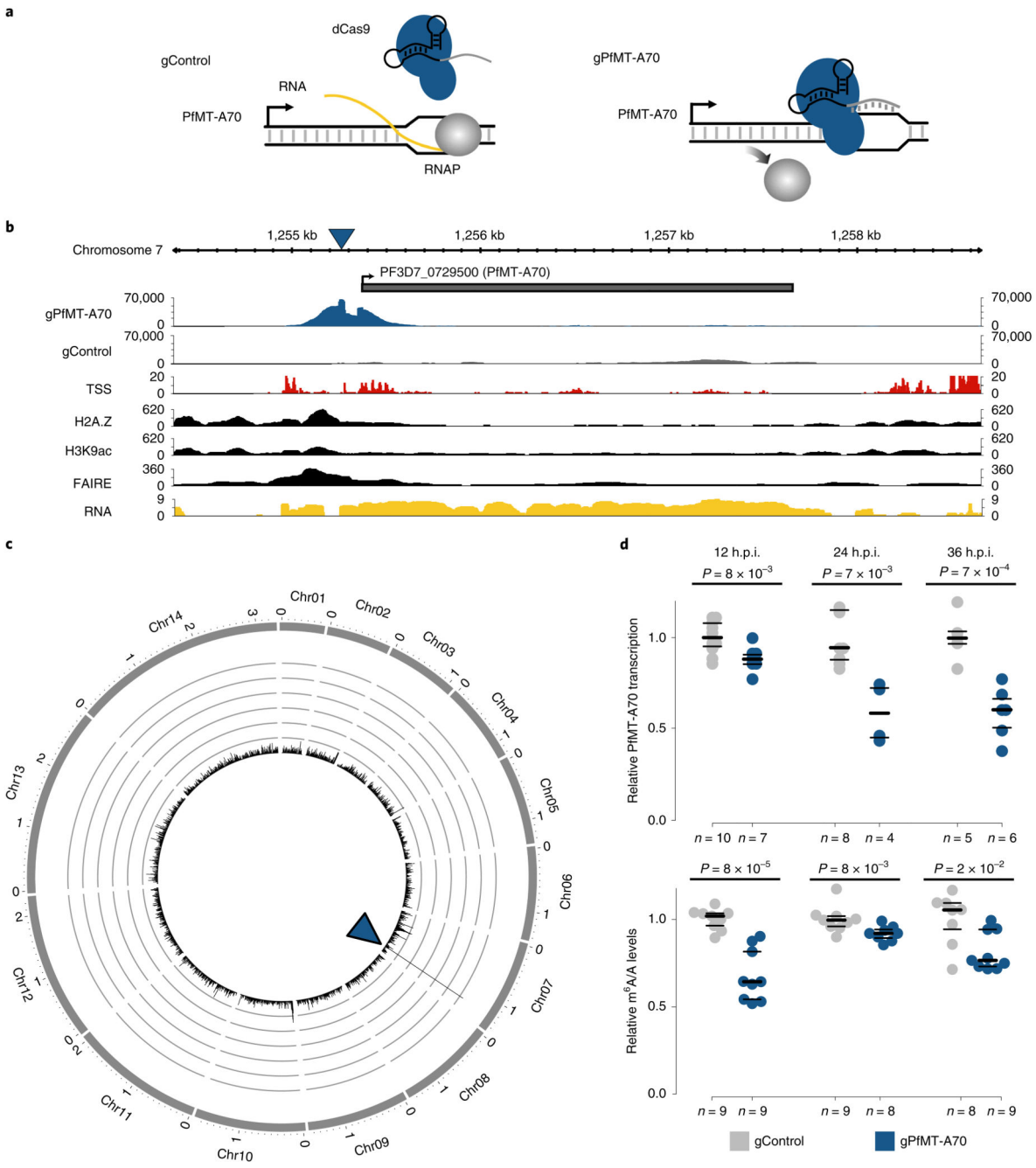

Fig. 3. Knockdown of the PfMT-A70 m^{6}A methyltransferase by CRiSPRi.

a, Diagram of the CRISPR interference system for targeted transcriptional knockdown of PfMT-A70. A non-specific gRNA (gControl) without a binding site in the *P. falciparum* genome is used as a negative control in all experiments (left). The specific gRNA (gPfMT-A70) targets the PfMT-A70 promoter on the non-template strand downstream of the putative transcription start site, blocking the elongating RNA polymerase II (RNAP) and silencing the target gene (right). **b**, dCas9-ChIP sequencing (12 h.p.i.) shows enrichment for gPfMT-A70-targeted dCas9 (blue), but not non-targeted dCas9 (gControl in grey) at

Europe PMC Funders Author Manuscripts

the targeted upstream region of the PfMT-A70 gene (indicated at the top with a grey bar). Arrow indicates direction of transcription. The blue triangle indicates the location of the gRNA target site. Genomic features investigated in previous studies that define the putative promoter region are shown below: transcription start site (TSS)[34], histone 2A variant (H2A.Z)[33], acetylation of histone H3 at lysine 9 (H3K9ac)[5], nucleosome depletion as determined by FAIRE-seq[32] (FAIRE), and RNA-seq coverage (RNA) at the genomic locus[6]. **c**, Circos plot of gPfMT-A70 dCas9 ChIP-seq (normalized to gControl) across all 14 nuclear chromosomes (exterior grey bars) shows no substantial enrichment of dCas9-binding other than at the PfMT-A70 promoter (blue arrowhead), demonstrating the high specificity of the method. Chromosome name and length (in megabases) are indicated at the exterior of the plot. The *y* axis indicates ChIP enrichment on a scale from 0 to 150 RPKM in 1,000 nt windows. dCas ChIP-seq data (**b**,**c**) are representative of two independent biological experiments. **d**, Comparison of PfMT-A70 transcription measured by RT-qPCR (top) and m^6A/A measured by LC-MS/MS (bottom) between gControl (grey) and gPfMT-A70 (blue) parasites at three different time points over the IDC (indicated at the top). PfMT-A70 transcript levels were normalized to those of the housekeeping gene serine tRNA ligase (PF3D7_0717700). The number of biological replicates is indicated on the bottom of the graph. *P* values were calculated using two-sided independent-samples *t*-test (RT-qPCR) and a two-sided Mann-Whitney *U*-test (LC-MS/MS). The average of PfMT-A70 transcription and m^6A/A levels in gControl parasites were set to 1. Horizontal lines represent median and interquartile ranges.

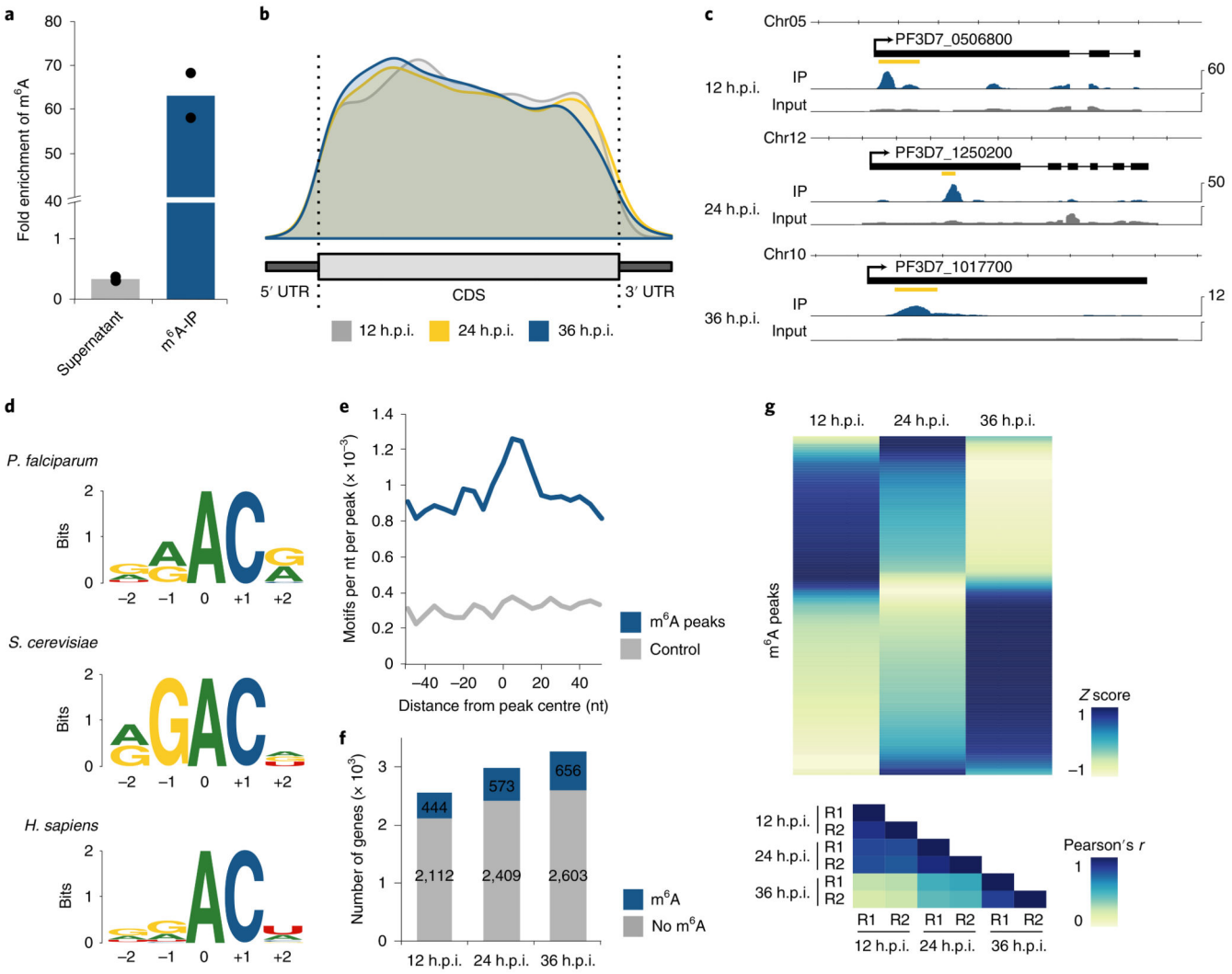

Fig. 4. Differential m^{6}A methylation during the *P. falciparum* iDC.

a, Fold enrichment of m^{6}A levels as measured by LC-MS/MS in different fractions of the m^{6}A-IP experiment, showing a three-fold depletion in the supernatant and 63-fold enrichment in the eluate. m^{6}A levels were normalized to the total number of adenosines (that is, m^{6}A/A) for each fraction, and fold enrichments were calculated as ratios over the m^{6}A/A levels in the input mRNA sample (collected at 36 h.p.i.). Points represent individual biological replicates, with bars showing the mean. **b**, Distribution of m^{6}A peak location along a normalized transcript coding sequence (CDS), 500 nt upstream of the start (5' UTR) and 500 nt downstream of the stop codon (3' UTR) for peaks identified at 12 (grey), 24 (yellow) and 36 (blue) h.p.i. The total number of identified m^{6}A sites by m^{6}A-seq is likely to be an underestimate. Besides those that were not called due to the conservative annotation approach, m^{6}A sites in transcripts reaching peak expression at different time points or sites in low complexity regions are likely to have been missed. **c**, Exemplary RNA sequence coverage of m^{6}A-IP (blue) and input (grey) gControl samples showing m^{6}A peaks identified at 12 h.p.i. in PF3D7_0506800 (transcription factor 25; RPKM, 107), 24 h.p.i. in PF3D7_1250200 (CSC1-like protein; RPKM, 53) and at 36 h.p.i.

in PF3D7_1017700 (conserved protein of unknown function; RPKM, 10). The location of the m^{6}A peak is indicated by the yellow bar. Data are representative of two independent biological experiments. **d**, Comparison of the deduced sequence motif of m^{6}A methylation sites in *P. falciparum* (top), *S. cerevisiae* (middle)[27] and human (bottom)[35]. The relative height of each nucleotide indicates frequency and the total height at each position represents sequence conservation ('bits'). The N^6-methylated adenosine is located at position 0. **e**, Density plot showing the occurrence of the consensus motif within ±50 nt of all significant m^{6}A-seq peak summits (blue) and size-matched random control sequences (grey) in 5 nt windows. **f**, Bar charts indicating the number of transcripts (RPKM ≥5) with no (grey) or at least one significant (blue) m^{6}A peak at three different time points over the IDC. **g**, Heatmap of average row *Z* score normalized m^{6}A enrichments in gControl parasites (average derived from $n = 2$ biologically independent experiments) displaying changes in transcript-specific methylation at three time points throughout the IDC (top). Each row represents an m^{6}A peak ($n = 840$) in a transcript expressed with RPKM ≥ 5 at all three time points. Bottom: heatmap showing Pearson's *r* correlation coefficients of m^{6}A enrichments, demonstrating a high degree of reproducibility between the two replicates (R1 and R2) at each time point. Blue indicates a high *Z* score while yellow indicates a low *Z* score (see Methods).

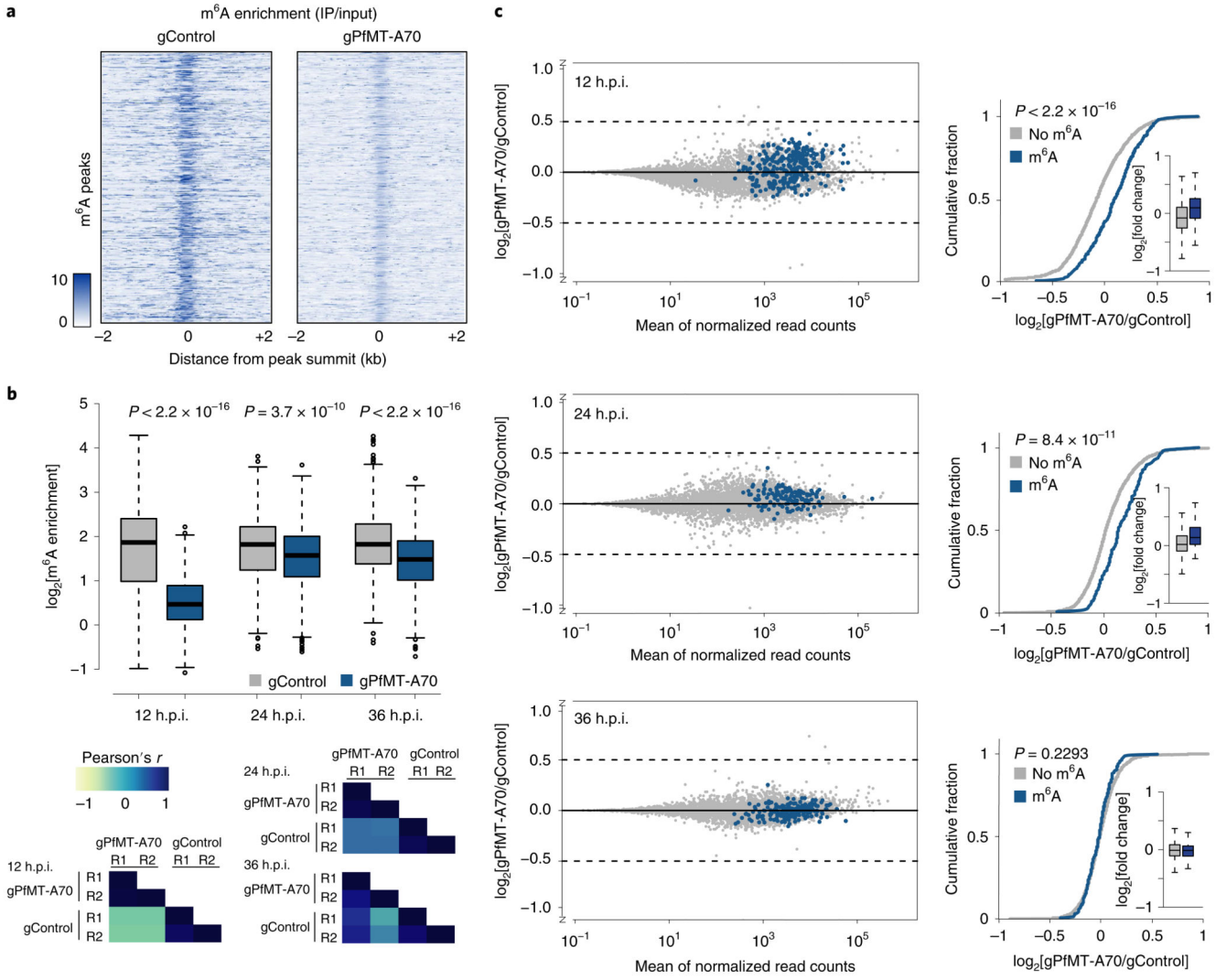

Fig. 5. PfMT-A70 knockdown leads to upregulation of m^{6}A-methylated transcripts.

a, Heatmap of m^{6}A enrichment at 12 h.p.i. depicting the decrease in m^{6}A enrichment for individual m^{6}A peaks (n = 603, y axis) between gControl (left) and gPfMT-A70 (right) parasites calculated in 10 nt windows in a region ± 2 kb around m^{6}A peak summits. Darker colour indicates higher enrichment. **b**, Boxplot of m^{6}A enrichment for all m^{6}A peaks in gControl (grey) and gPfMT-A70 (blue) parasites showing a significant decrease in m^{6}A enrichment following PfMT-A70 depletion at all three time points. m^{6}A enrichment for each peak was averaged over two replicates in each condition and time point (see correlation between replicates below). Number of m^{6}A peaks: 603, 873 and 996 at 12, 24 and 36 h.p.i., respectively. Centre line, median; box limits, first and third quartile; whiskers, 1.5× interquartile range. P values were calculated using a two-sided Mann-Whitney U-test. Bottom: heatmap depicting Pearson's r correlation coefficients of m^{6}A enrichment among replicates of gControl and gPfMT-A70 parasites at all three time points (see Supplementary Tables 4–6). Blue indicates a high score while yellow indicates a low score. **c**, MA-plots (left) of log$_2$[gPfMT-A70/gControl, M] plotted over the mean abundance of each gene (A)

at 12 (top), 24 (middle) and 36 (bottom) h.p.i. $n = 3$ for gPfMT-A70 and $n = 2$ for gControl at all time points. Transcripts containing m^6A peaks with a more than two-fold decrease in m^6A enrichment following PfMT-A70 depletion are highlighted in blue. Cumulative fraction plots (right) comparing the distribution of $\log_2$[gPfMT-A70/gControl] between non-methylated transcripts (grey; $n = 2{,}131$, 3,208 and 3,334 at 12, 24 and 36 h.p.i., respectively) and transcripts with a more than two-fold decrease in m^6A enrichment following PfMT-A70 depletion (blue; $n = 284$, 132 and 199 at 12, 24 and 36 h.p.i., respectively) at 12 (top), 24 (middle) and 36 (bottom) h.p.i. *P* values were calculated using a two-sided Mann-Whitney *U*-test. Insets: boxplots comparing the $\log_2$ fold-changes between the two classes of transcripts. Centre line, median; box limits, first and third quartile; whiskers, 1.5× interquartile range.

Europe PMC Funders Author Manuscripts

Europe PMC Funders Author Manuscripts

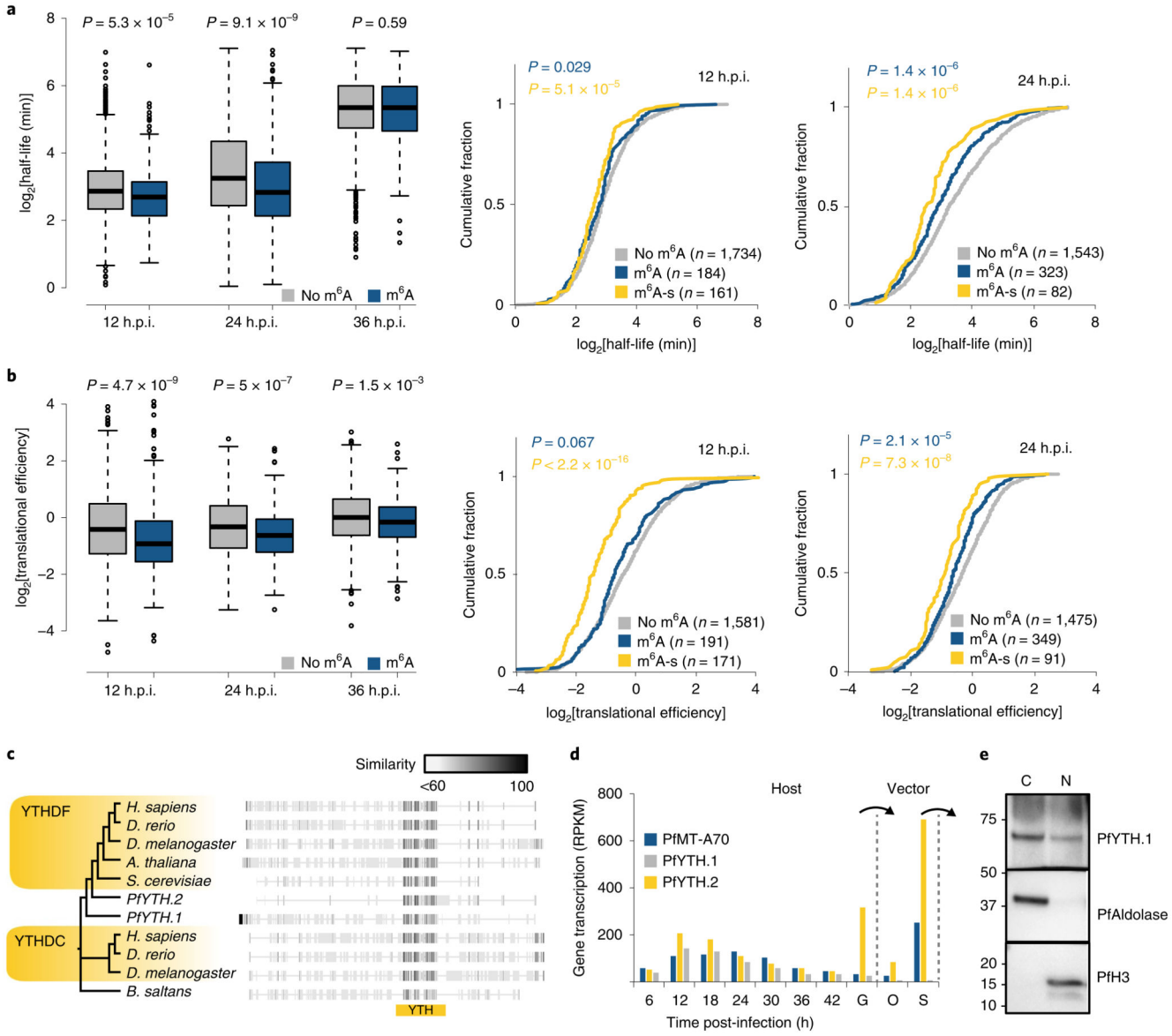

Fig. 6. Correlation of m^{6}A with mRNA stability and translational efficiency.

a, Boxplots (left) depicting mRNA half-lives for transcripts without (grey; n = 1,734, 1,534 and 1,495 at 12, 24 and 36 h.p.i., respectively) or with (blue; n = 301, 377 and 383 at 12, 24 and 36 h.p.i., respectively) m^{6}A peaks at 12, 24 and 36 h.p.i. Centre line, median; box limits, first and third quartile; whiskers, 1.5× interquartile range. P values were calculated with a two-sided Mann-Whitney U-test. Right: cumulative fraction plots of mRNA half-lives at 12 and 24 h.p.i. for transcripts without m^{6}A peak (grey), with m^{6}A peak (blue), and 'm^{6}A-sensitive' (yellow) transcripts. P values were calculated with a two-sided Mann-Whitney U-test against mRNA half-lives of non-methylated transcripts. **b**, Boxplots (left) depicting translation efficiencies for transcripts without (grey; n = 1,584, 1,475 and 1,486 at 12, 24 and 36 h.p.i., respectively) or with (blue; n = 317, 412 and 435 at 12, 24 and 36 h.p.i., respectively) m^{6}A peaks at 12, 24, and 36 h.p.i. Centre line,

median; box limits, first and third quartile; whiskers, 1.5× interquartile range. *P* values were calculated with a two-sided Mann-Whitney *U*-test. Right: cumulative fraction plots of translation efficiencies at 12 and 24 h.p.i. for transcripts without m^6A peak (grey), with m^6A peak (blue), and 'm^6A-sensitive' (yellow) transcripts. *P* values were calculated with a two-sided Mann-Whitney *U*-test against translation efficiencies of non-methylated transcripts. **c**, Phylogenetic tree and protein alignment of the putative m^6A reader protein PfYTH and orthologues in other eukaryotes. The location of the YTH domain is indicated below (yellow bar). The grey scale gradient indicates the percentage similarity across all proteins at an aligned position. YTHDC, YTH domain-containing protein; YTHDF, YTH domain-containing family protein. **d**, Transcription (RPKM) of the *P. falciparum* PfYTH proteins and PfMT-A70 over the course of the IDC[6], stage V gametocytes (G), oocysts (O) and salivary gland sporozoites (S). Arrows indicate transmission from host to vector and vice versa. **e**, Western blot analysis showing the enrichment of HA-tagged PfYTH in the cytoplasmic (C) and nuclear (N) fractions at 12 h.p.i. PfAldolase and histone H3 serve as controls for the cytoplasmic and nuclear fractions, respectively. Numbers on the left indicate molecular weight in kilodaltons. Data are representative of two independent biological experiments.

Europe PMC Funders Author Manuscripts